Master RADMEP

Master *Radiation and its Effects on MicroElectronics and Photonics Technologies* (RADMEP)

Quantitative Analysis of Optical Parameters Using THz-TDS

Master Thesis Report

Presented by

Aditya RAJ

and defended at

University Jean Monnet

11/12 September 2023

Academic Supervisor: Prof. Adriana Morana

Host Supervisor: Dr. Romain PERETTI

Host Co-Supervisor: Dr. Noureddin OSSEIRAN

Jury Committee: Prof. Arto Javanainen, University of Jyväskylä

Prof. Paul Leroux, KU Leuven, Geel campus

Prof. Sylvain Girard, Université Jean Monnet

Prof. Frédéric Saigné, University of Montpellier

Erasmus+

Quantitative Analysis of Optical Parameters Using THz-TDS

Master Thesis Report

Aditya Raj

September 2023

Master Radiation and its Effects on MicroElectronics and Photonics technologies (RADMEP)

Abstract

Terahertz Time Domain Spectroscopy gained much popularity in recent decades due to its broadband range and high signal to noise ratio. Researchers have already started working rigorously on all aspects of this domain from developing spectroscopy for getting high-resolution signal to extracting other indispensable information out of gas molecules and biological samples. In this study, I have emphasize the use of this powerful THZ-TDS technique to extract information in a quantitative approach. We have shown that the sensitivity of our spectroscopy can be estimated by measuring the concentration of a sample. This has been demonstrated through a physical model applied on both solid samples as well as on gas sample.

In addition, knowing that several convolutional mathematical physical modelling are being exploited in order to acquire better precision but less work has been done on measuring the uncertainty on the parameters extracted from these mathematical modelling. In this study, I have also attempted to visualise uncertainties on optical parameters of lactose sample extracted through Lorentz model of electronic dispersion. This is achieved by numerically evaluating Hessian matrix, which is a second order partial derivatives of the function at optimised parameters. Subsequently, the standard deviation is computed by taking diagonal elements of inverse of this Hessian matrix. This uncertainties are shown using error bars on real and imaginary part of refractive index of lactose sample.

Acknowledgement

First, I want to express my cordial gratitude to my supervisor Dr. Romain PERETTI who gave me this auspicious opportunity to work under his experienced leadership. I thoroughly remember his golden words that fetched me into the right direction for this project. I still remember him saying to think like a researcher rather than a student. He motivated me to think independently, out of the box and not to be scared to start something new by my own.

I would like to extend my gratitude to my co-supervisor Dr. Noureddin OSSEIRAN for constantly guiding me throughout the internship. The best part of him, which I appreciate the most, is his way of pushing me to be independent and learn by myself. Apart from this, I would like to acknowledge all the members of the Terahertz-Photonics group at IEMN, Lille. I would like show special acknowledgement to Sophie ELIET and Jeyan BICHON.

In this master's thesis, I had to take measurements using the Four-point probe instrument kept in the clean room. I successfully took all the measurements and this could not have been possible without the support of Victor MERUPO and proper training and guidance by Jérémie CHAILLOU.

I would like to show regards to all the people associated with E+EMJMD RADMEP programme. I cannot forget the motivation and guidance given by Prof. Sylvain GIRARD, Adrian MORANA and Prof. Matteo FERRARI at every step during the journey of this prestigious Master's degree.

At the end, I cannot forget to mention my family and friends who backed me up whenever I felt down. I remember the day when I almost shed tears while talking to my mother on phone sharing my doubt if I am the right person for research. Without any hesitation, she reminded me how I came this far on my own, achieving what is still a dream for millions. I would like to give special acknowledgement to my friends Afrina HASAN, Mohit PATEL and Rukhsar SAYYED for constantly helping in taking right decisions throughout this internship journey.

Table of Contents

List of Abbreviation

THz	Terahertz
TDS	Time Domain Spectroscopy
PC	Photoconductive
EM Wave	Electromagnetic Wave
E field	Electric field
H field	Magnetic field
DFM	Difference Frequency Mixing
OR	Optical Rectification
PA	Photoconductive Antenna
Si	Silicon
DC	Direct Current
AIC	Akaike Information Criterion
FP	Fabry-Perot
cm	centimetre
Ref	Reference
Fig	Figure
w/w	weight/weight
mg	milligram
mbar	millibar
etc.	et cetra

Table of Figures

List of Tables

1. Introduction

Acknowledging the limits of fluctuation of the data, whether it is extracted from experimental setups or mathematical simulations, has consistently held significance in research community on par with the data that are actually extracted. This master's thesis sheds light on quantitative analysis of optical parameters procure through mathematical modelling using Terahertz Time Domain Spectroscopy. In the present chapter, I will start with the general aspects of radiation-matter interaction and the foundation of spectroscopy in terahertz domain, and then the idea of spectroscopy in time domain is discussed. Finally, the overview of the manuscript's structure will be provided.

1.1. Radiation-Matter Interactions: Foundation of Spectroscopy

The first glimpse of spectroscopy was seen way back in 17th century when Issac Newton demonstrated the dispersion of sunlight through prism, which he coined the term 'spectrum' for the mixture of all colours of the rainbow [1]. Later the theory was built and developed by other pioneering scientists like William Hyde Wollaston (1766–1828), Joseph von Fraunhofer (1787–1826), and later Ritter von Fraunhofer [2]. Spectroscopy, in general, is a field of science that exploits the interaction between electromagnetic radiation and matter. It is based on the measurement and interpretation of spectra acquired at different frequencies or wavelengths [3]. When light interacts with matter, several physical mechanism occurs like reflection, absorption, scattering, transmission or emission depending on the type and nature of material and the properties of light. Spectroscopy involves study of these interactions to extract useful information about material like its composition, molecular or atomic structure, electronic transition and more. This further help us to understand several chemical and physical properties of the material. Spectroscopy is a broad field and classified as different methods depending on type of radiative energy, nature of interaction and type of material. In this study, we are working with the radiative energy falls in Terahertz range. This is discussed in next section.

1.2. Spectroscopy in Terahertz Range

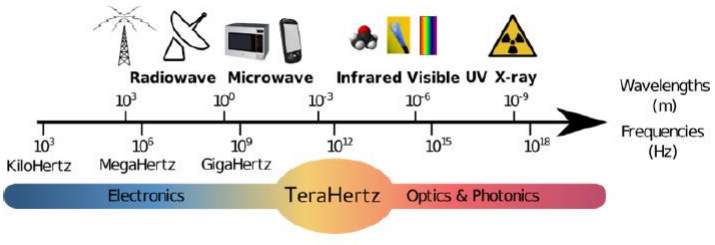

Fig 1: Illustration of THz domain in Electromagnetic spectrum. Figure taken from [4].

Terahertz range, or far-infrared (between 100 GHz and 10 THz or 0.3cm^{-1} to 333cm^{-1}) is the least explored EM spectrum in the research community. This region of the EM spectra is usually called the THz gap, and this is mainly due to lack of powerful THz generation sources. In fact, the THz region falls in the limit between the optical sources of the infrared and the electronic sources of the microwave region. In the last few decades, the THz domain witnessed great enhancement in generation sources, especially with the advancements in ultra-fast lasers and frequency combs [5], [6].

Terahertz wave can be generated using several methods including frequency mixing, optical rectification using nonlinear optics and photoconductive antennas [7]. Generation of Terahertz wave using difference frequency mixing (DFM) uses two lasers having frequency difference in THz range. The advantage of this method is that it is highly tuneable and spectral resolution up to 1 MHz. Optical rectification is a technique for the generation of Terahertz wave where nonlinear crystal is used. The OR involves second order nonlinear process preferable for the generation of strong single cycle THz wave [8]. Photoconductive Antennas also called as "Auston Switch" is one of the first and oldest techniques for the generation of THz wave [9]. PA is widely used because of its several advantages over others like low maintenance, broadband, low cost, compact and efficient. Basic setup for THz wave generation using PA is discussed in later section below.

1.3. What is Terahertz Time Domain Spectroscopy?

Terahertz Time Domain Spectroscopy itself is a versatile technique in research field. It has wide applications in chemistry, biology, material sciences, chemical imaging and other industries [4]. The basic principle of THz-TDS is shown in the figure below. Ultra-fast (femtosecond) laser beam is split into two beams. One of it is used to generate THz wave and the other is used for detection after passed through delay line for sampling of signal in time domain. THz-TDS measures the time taken by the radiation to travel through the material after interacting with the sample material. Therefore, by studying the pulse's amplitude and phase, researchers can extract the salient information about the material's composition, structure, and properties.

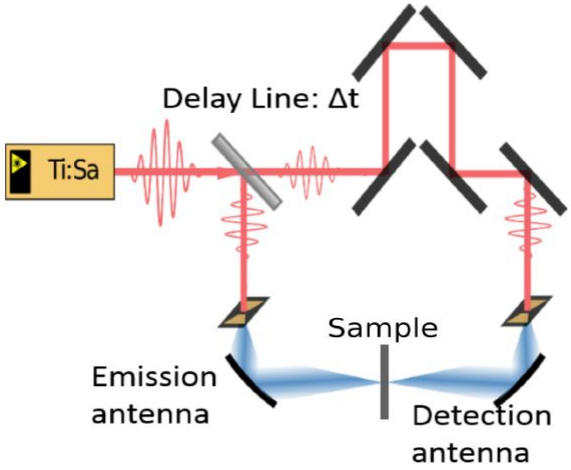

Fig 2: Schematic of the principle of THz-TDS. Figure taken from [4].

1.4. Generation of THz wave using PA

Terahertz PC antenna consist of two closely spaced metal strips implanted into a semiconductor substrate consisting charge carriers with a very short lifetime. These metal strips are given a DC bias voltage across them. When a sharp ultra-fast photon having energy greater than the band gap of the semiconductor, hits the semiconductor between the metallic gaps, electron-hole pairs are generated. These generated electron hole pair is then accelerated by the bias voltage and subsequently current density decline rapidly, giving rise to a very fast potential change. This induces oscillation in the antenna and in turn terahertz radiation is generated. The resultant terahertz radiation is emitted in wide direction. The radiation is then collimated using a converging mirror or lens to get a uniform signal.

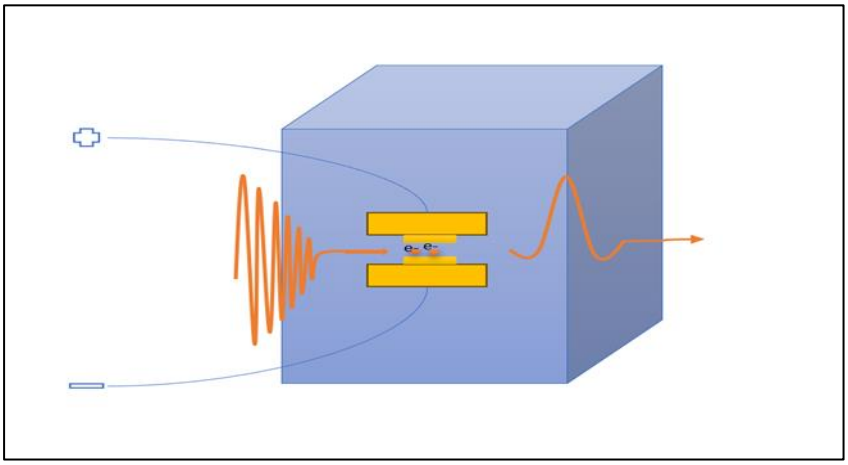

Fig 3: Schematic of generation of THz radiation.

1.5. Detection of THz wave using PA

Detection of terahertz radiation is based on same principle as the generation. In this case the metallic strips are not connected with bias voltage but are connected with current measuring device. So, when the terahertz radiation strikes the semiconductor containing charge carriers already generated by laser pulse, these are accelerated by this THz radiation. In this way the whole THz wave is mapped with photocurrent in time domain by delaying the time between THz wave and photocurrent. The current is converted to voltage with a high gain to measure the weak signal properly. In addition a lock in amplifier can be used to enhance the signal to noise ratio.

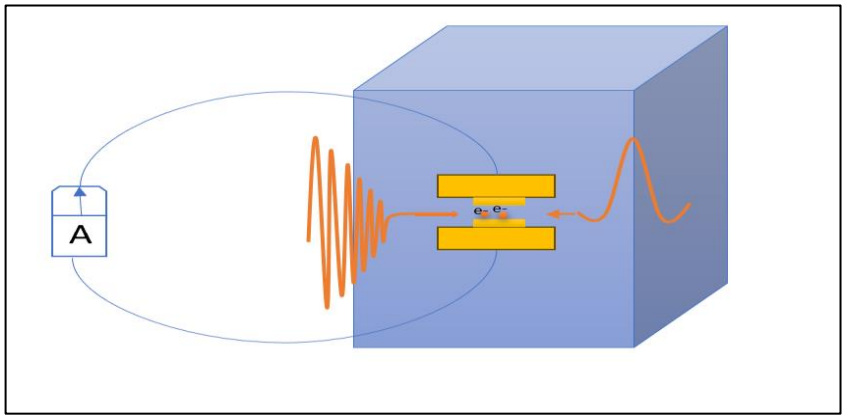

Fig 4: Schematic of detection of THz radiation.

As stated before the sampling of the detected THz wave is done by the computer controlled very fast mechanical delay line. It consist of retroreflective mirror and allows to record the temporal variation of photocurrent. The sampling time when path length, Δx is known, is given by [4]:

$$\Delta t = \frac{2\Delta x}{c} + \tau(t) \qquad (1)$$

Where, c is the speed of light in vacuum and τ is the sampling error due to positioning of the retroreflective mirror.

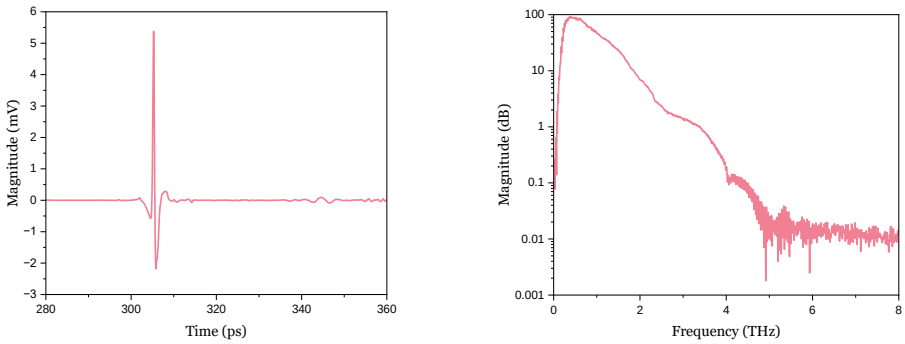

Fig 5: THz signal in time domain and its Fourier transform. The signal is detected inside a nitrogen-purged box without any sample in between antennas.

As explained above, the collected experimental data is a time-reconstructed THz pulse. In order to better understand the usefulness and applicability of these kind of data, a brief theoretical description is given in what follows, to help understand the basis of data analysis in our experiments.

1.6. Maxwell's' Equations

Any wave on electromagnetic spectrum is governed by Maxwell's equations. The four equations that describe the relation between E and H field and their behaviour are

$$\nabla \cdot D = \rho_f \tag{2}$$

$$\nabla \cdot B = 0 \tag{3}$$

$$\nabla \times \mathrm{E} = -\frac{dB}{dt} \tag{4}$$

$$\nabla \times \mathrm{H} = \frac{dD}{dt} + J \tag{5}$$

Where D is the displacement field, B is the magnetic field, E is the electric field, H is the magnetising field, J is the current density, $\nabla \cdot$ and $\nabla \times$ are the divergence and curl of the field respectively and $\frac{d}{dt}$ is time derivative of the field. Considering material is nonconductive and current density is zero i.e. $\rho_f = 0$ and $J = 0$, we have the electric component of wave equation

$$\nabla^2 \mathrm{E} = \mu_0 \mu_r \varepsilon_0 \varepsilon_r \frac{\partial^2 E}{\partial t^2} \tag{6}$$

Where, μ_o is the permeability of the free space, μ_r is the relative permeability; ε_o is the permittivity of the free space and ε_r is the relative permittivity.

Also, we know that, speed of light in medium is given by $c = 1/\sqrt{\varepsilon\mu}$ and refractive index $n = \sqrt{\varepsilon_r}$. So, our wave equation becomes ($\mu_r = 0$),

$$\nabla^2 E = \frac{n^2}{c^2} \tag{7}$$

So, the solution of plane wave linearly polarized having single frequency ω is given by:

$$\vec{E}(z,t) = E^0 e^{j(kz-\omega t)} \tag{8}$$

Having $k = 2\pi/\lambda$ as wave vector, k can be written as a function of frequency ω as follows:

$$k^2 = \frac{n^2}{c^2}\omega^2 \tag{9}$$

So, any planar wave is characterized by an attenuation in amplitude and delay in phase of the field when travelling through any medium. Or in other words, if we have given a wave equation, and at any given frequency, one can extract optical parameters like the complex refractive index

1.7. Transfer function

An electromagnetic (EM) wave, when passing through any medium is submitted to attenuation and phase delay along the field of the wave. The complex transfer function describes the behaviour of propagating wave upon interacting with a system by comparing the signal before and after passing through the sample [10]. Assuming working in linear optics, mathematically, the complex transfer function is given by:

$$\tilde{T}(\omega) = \frac{\tilde{E}_{Sample}}{\tilde{E}_{Ref}} \tag{10}$$

We can break down the transfer function into its constituent components like Fresnel's coefficient for interface between two materials, propagation term throughout the sample and Fabry–Perot term for multiple reflections inside the sample [10] .

$$\tilde{T}(\omega) = \tilde{s}(\omega) \times \exp\left(-j\frac{\omega d}{c}(\tilde{n}(\omega) - 1)\right) \times \widetilde{FP}(\omega) \tag{11}$$

Here, $\tilde{s}$ is the Fresnel coefficient at normal incidence between the air medium interfaces. Given by,

$$\tilde{s}(\omega) = \tilde{t}_{1\to2} \times \tilde{t}_{2\to1} = \frac{4\tilde{n}(\omega)}{(\tilde{n}(\omega) + 1)^2} \tag{12}$$

The complex transfer function provides the relation between input and output EM wave that passes through a dispersive medium, experiences attenuation and phase shift. Therefore, it gives important information about the sample in terms of absorption coefficient and refractive index as a function of frequency, in addition to an extensive set of other spectroscopic and materialistic parameters.

In order to extract as much information as possible from the measured time-domain data, and as described in [10], it is possible to fit the experimental data to several models depending on the nature of information available, as well as the interest in the application of the sample under study. In what follows, you can find a description of the different models used in this work.

1.8. Dispersive models

When a dynamic electric field passes through a medium, it induces the polarization of this medium. Depending on the type of the material and frequency of the field, the mechanism of polarization could be dipolar, ionic or electronic.

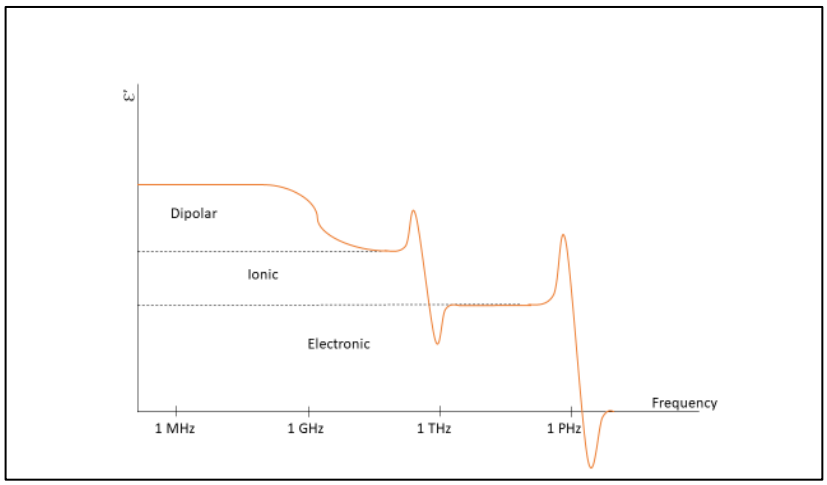

Fig 6: Variation in real part of dielectric constant with frequency.

To understand the frequency dispersion of permittivity of the material, we generally use simple mathematic functions or models. Using these models, we can get information about the optical properties of the material. Some of the models to study dispersion are Debye's 1st and 2nd order model, Drude model and Lorentz model. In this study, we are going to employ Drude and Drude-Lorentz models, which can describes the permittivity in complex plane and help to relates the dielectric constant to the motion of the charges in the material.

1.8.1. Drude Model

Drude model is a well-known dispersive model for materials containing free electrons like metal and doped semiconductor. This model was purposed by a famous physicist Paul Drude. With the assumption of non-interacting free electrons and motionless positive ions in metal and semiconductors [11], [12], Drude model for polarization and dielectric constant is widely applicable, and shows good agreement with the experimental data in general. In this mode, the permittivity of the material is given by:

$$\tilde{\varepsilon} = \tilde{\varepsilon}_{\infty} + \frac{\omega_p^2}{\omega^2 + j\omega\gamma_p} \tag{13}$$

Here, $\tilde{\varepsilon}_{\infty}$is permittivity at the highest frequency ($\tilde{\varepsilon}_{\infty} = 1$), ω_p is electron plasma frequency and $\gamma_p$is the damping rate of plasma electrons. This equation shows the interaction of incoming radiation with plasma and changes the dielectric property of the medium.

Also, given by the Ohm's law, we can derive the conductivity of the medium knowing the current density. At, DC current, the conductivity is given by,

$$\sigma = \frac{\varepsilon_0 \omega_p^2}{\gamma_p} \tag{14}$$

Given the value of plasma frequency and damping of plasma electrons, we can calculate the conductivity (or resistivity) of metals and semiconductors [13] .

1.8.2. Drude-Lorentz Model

The behaviour of electric field through any dispersive material can be studied using Drude-Lorentz model. Paul Drude initially proposed this model in 1900 for electrical conduction and later in 1905, Hendrik Antoon Lorentz extended it. The permittivity of the material in this model is given by the following equation:

$$\tilde{\varepsilon} = \tilde{n}^2(\omega) = \tilde{\varepsilon}_{\infty} + \frac{\omega_p^2}{\omega^2 + j\omega\gamma_p} + \sum_{k=1}^{k_{max}} \frac{\Delta\varepsilon_k \omega_{0,k}^2}{\omega_{0,k}^2 - \omega^2 + j\omega\gamma_k} \tag{15}$$

Where, $\Delta\varepsilon_k$ is the line strength of the Lorentz oscillator, ω_0 is the Lorentz oscillator and γ_k is the damping rate of the oscillator.

The change in the real part of dielectric constant is directly related to the change in the refractive index with frequency. This is known as dispersion as describe in the Fig 6. The imaginary part of the dielectric constant peaked at Lorentz frequency ω_0 describes the

Lorentzian line shape having the width proportional to the damping coefficient. This give rise to energy dissipation and called absorption.

1.9. Conclusion

In this section, we outlook the general aspects of radiation-matter interaction and how we can utilise this knowledge in spectroscopy to extract useful information of the material [14]. We describe the working principle of Time Domain spectroscopy in Terahertz range. To study the insight of the material when radiation penetrate through it, we make use of several mathematical model that describes this dispersion. In the upcoming section, we will demonstrate the implication of these models to extract optical information of the samples. In addition, we will introduce a method that will assist us to quantify the uncertainties on our extracted parameters.

2. Information Extraction for Silicon Wafer Samples Using THz-TDS

2.1. Introduction

Silicon Wafer has profound significance in material science and electronics because of its crystal structure, mechanical properties and surface chemistry. Silicon is considered as the simplest sample to understand the THz wave-matter interaction and study the Drude model for dielectric constant. It shows great transmission properties within the THz range with relatively low absorption and minimal dispersion [15]. In the work done in [15], authors shows the transmission characteristics of Si wafer samples consisting different resistivity. They showed that the wafer with low conductivity shows lower THz transmission compared to the wafer with high conductivity. In this study I tried to quantified the resistivity from Si wafer having different thickness and carrier concentrations. The experimental setup is shown in the left side of Fig 7. The sample is carefully aligned perpendicular to the direction of the wave to avoid any inconsistency in the optical thickness and Fabry-Perot echoes from it. Since we are working with the transmission spectra of THz wave, the samples were chosen in such a way that enough power of THz wave is passing through it. As shown in right side of Fig 7, transmitted E-field in time scale for different sample and its comparison with reference signal.

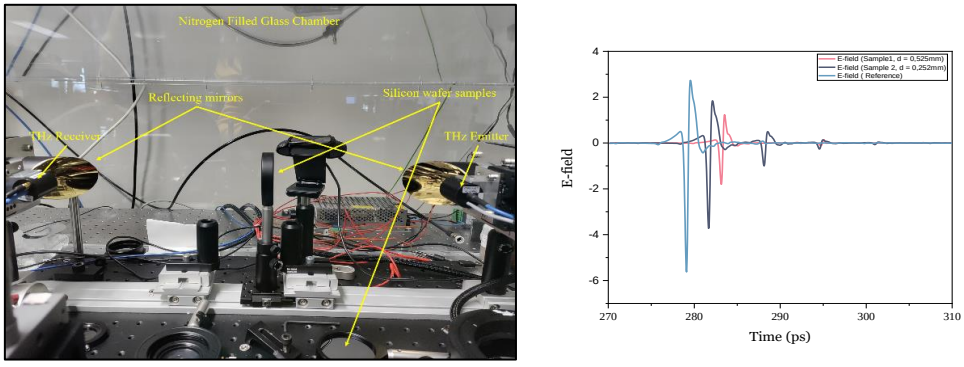

Fig 7: Left : Experimental setup for silicon wafer, Right : Comparison of THz pulse intensities for different samples.

From the graph shown in Fig 7, we see that the intensities of the wave decreases as we put the sample in between the THz wave due to absorption inside the sample. Also as we increases the thickness of the sample, the intensity of the E-field decreases showing the variation of conductivity and in other words, variation of electron density in the samples. In the later section of this chapter, we will show the evaluation of the number of charge carriers present in the sample using the parameters extracted from FIT@TDS. Now, in the next section fitting of experimental data for three samples is discussed.

2.2. Experimental Setup

The experimental setup used in this experiment to measure transmission spectra of Si wafer is shown in the Fig 7. It consists of two antennas: one at the right end to emit THz radiation and one at the left end to detect THz radiation. The radiation is collimated by two parabolic mirror placed immediately after the antennas. The samples to be

measured are placed in between these reflecting mirrors. Since, the size of the samples (in our case 2 inch) are larger than the size of the collimated beam, we didn't required any lenses to focus down the beam on to the sample. The whole setup is placed inside the nitrogen purged glass box to avoid contact with water molecules.

2.3. Characterisation of Si wafer samples using FIT@TDS

We are using three Si wafer as our samples, each with different sizes and thicknesses. The samples does not contain any absorption line in our probed terahertz region (0.2-6 THz). Therefore, the Drude model was chosen to fit the experimental data for the samples.

2.3.1. 520 µm Si wafer sample

The fitted Electric field spectrum in frequency domain for this sample is shown in Fig 8 and its corresponding fitted real and imaginary part of refractive index are shown in Fig 9.

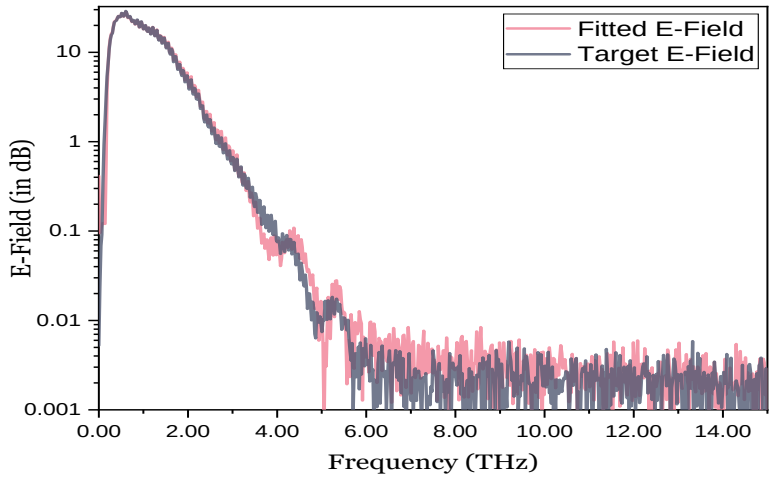

Fig 8: E-field spectrum in frequency scale from FIT-TDS for 520-µm Si wafer sample.

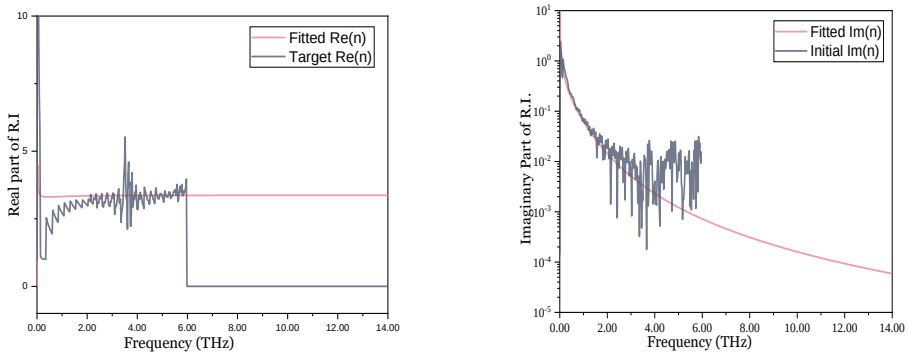

Fig 9: Simulated as well as Target Real and Imaginary part of R.I for 520-µm Si wafer sample.

All the initial and optimised value for parameters are tabulated below. Initially we did not include the noise matrix with an assumption that the noises are uncorrelated to save computational time. The noise envelop is used as the weighting function to fit the model. However, in the previous experiment, the group demonstrated that the usual assumption of non-correlated noise was not met in our system. Most of the noise was associated with the receiver end in the absence of THz signal. Moreover after further analysis on the noise it shows that these noises were proportional to the derivative of the signal. The group developed a software called correct@TDS using python programming language to correct the noises corresponding to fluctuation in the laser amplitude and thermal drift in the delay line [16], [17]. Now, we extracted the noise correlation matrix (precision matrix) which has the information not only about the magnitude of the noise but also corelation with the signal. This is then multiplied with error function for better fit [18]. We also tabulated the updated parameters after adding noise matrix in the fitting process.

Parameters	Initial guess value	Optimised value	Optimised value after adding noise matrix
ε_∞	11	11.3	11.3
ω_p *(Hz)*	2×10^{12}	5.8×10^{12}	5.6×10^{12}
γ_p *(Hz)*	7×10^{12}	8.2×10^{12}	7.9×10^{12}

Table 1: Fitting parameters with their initial guess and optimised value

2.3.2. 280 µm Si wafer sample

Similarly, The fitted Electric field spectrum in frequency domain for this sample is shown in Fig 10 and its corresponding fitted real and imaginary part of refractive index are shown in Fig 11.

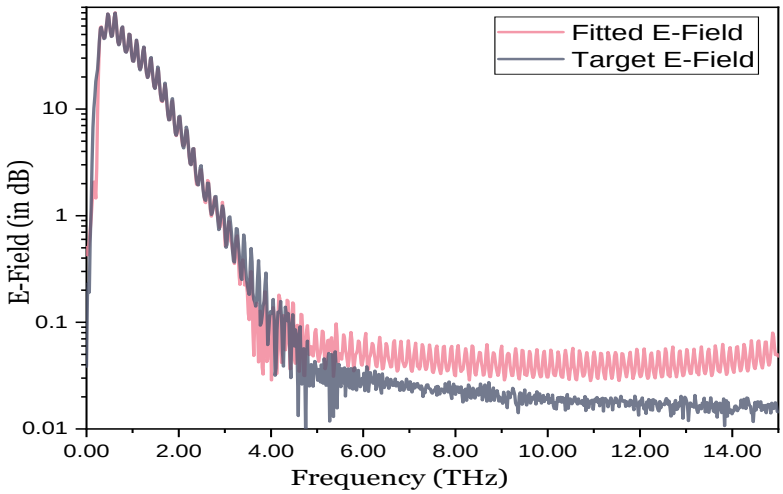

Fig 10: E-field spectrum in frequency scale from FIT-TDS for 280-µm Si wafer sample.

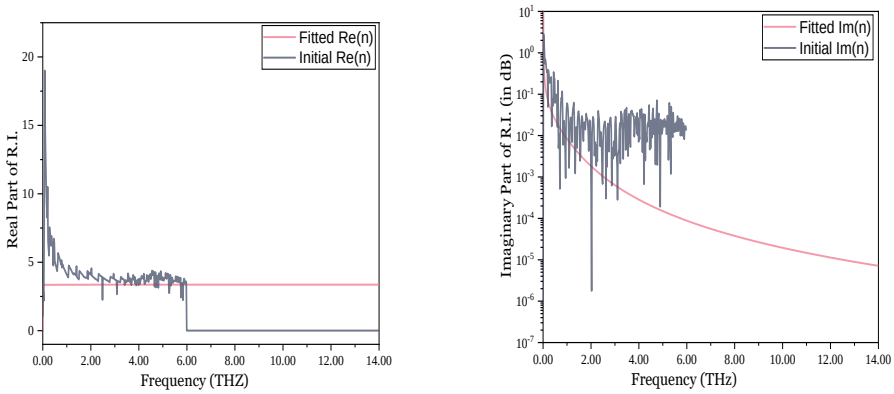

Fig 11: Simulated as well as Target Real and Imaginary part of R.I for 280-µm Si wafer sample.

This sample was thinner than the previous sample and all the values for fitting parameters are tabulated below.

Parameters	Initial guess value	Optimised value	Optimised value after adding noise matrix
ε_∞	10.9	11.2	11.3
ω_p *(Hz)*	2.2×10^{12}	2.1×10^{12}	2.2×10^{12}
γ_p *(Hz)*	7.8×10^{12}	7.4×10^{12}	7.9×10^{12}

Table 2: Fitting parameters with their initial guess and optimised value.

2.3.3. 290 µm Si wafer sample

This is another silicon wafer sample with comparatively same thickness as previous sample but with comparatively low resistivity. The fitted Electric field spectrum in frequency domain for this sample is shown in Fig 12 and its corresponding fitted real and imaginary part of refractive index are shown in Fig 13.

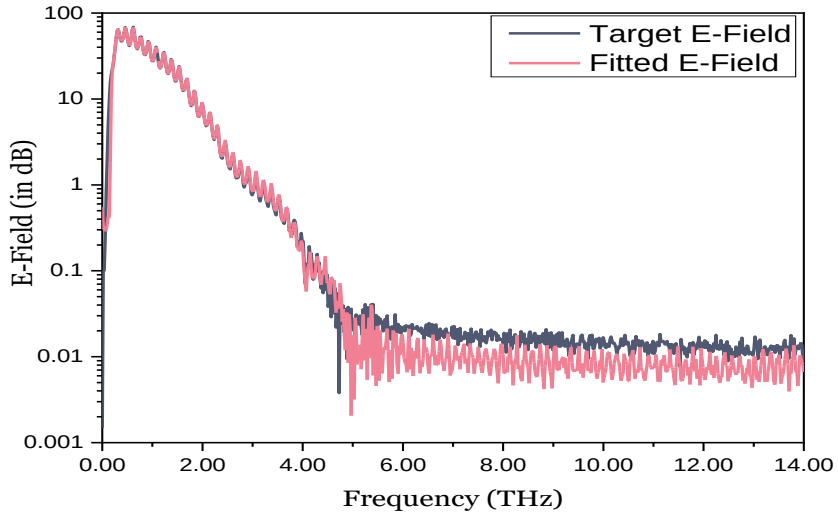

Fig 12: E-field spectrum in frequency scale from FIT-TDS for 290-µm Si wafer sample.

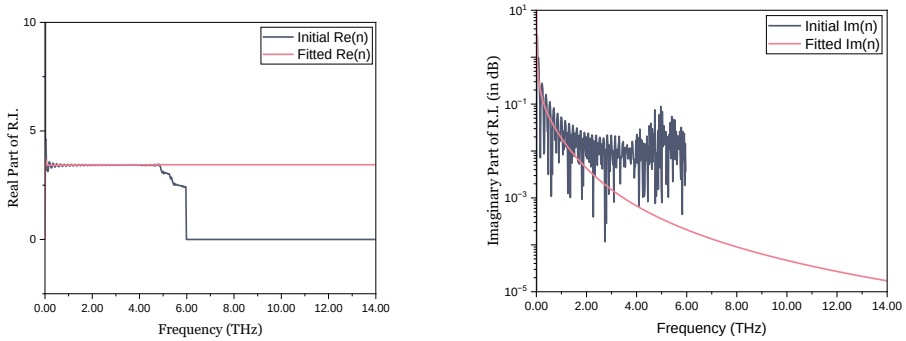

Fig 13: Simulated as well as Target Real and Imaginary part of R.I for 290-µm Si wafer sample.

Finally, the initial values for fitting parameters and their corresponding simulated optimised values are tabulated below.

Parameters	Initial guess value	Optimised value	Optimised value after adding noise matrix
ε_∞	10.6	11.8	11.8
ω_p *(Hz)*	5.0×10^{12}	3.2×10^{12}	3.2×10^{12}
γ_p *(Hz)*	7.0×10^{12}	7.6×10^{12}	7.7×10^{12}

Table 3: Fitting parameters with their initial guess and optimised value.

2.4. Resistivity calculation using Drude model using THz-TDS and comparison with Four-point probe method

As we discussed earlier, the Drude model of permittivity gives us fairly good idea about the conductivity of metals in the far-infrared (IR) spectral range [19]. It estimates the number of free electrons inside the metal that interacts with the radiation. Knowing this

we can easily estimate the conductivity of any metal provided that we have much information about the constituent parameters. However, in this study we are working on semiconductors having comparatively higher charge carriers.

As discussed in page 7, the permittivity of a material from Drude model is given as:

$$\tilde{\varepsilon} = \tilde{\varepsilon}_{\infty} + \frac{\omega_p^2}{\omega^2 + j\omega\gamma_p} \tag{16}$$

So, the question arises that, is it possible to extract more information out of it if we could know plasma frequency, ω_p and damping rate of plasma frequency, γ_p. So, the answer is yes. After proper derivation of equation of motion of free electrons under Electric field and applying ohm's law, we have the conductivity of material given as:

$$\tilde{\sigma}(\omega) = \frac{i\omega\varepsilon_0\omega_P^2}{\omega^2 + i\omega\gamma} = \frac{\varepsilon_0\omega_P^2\gamma}{\omega^2 + \gamma^2} + i\frac{\omega^2\varepsilon_0\omega_P^2}{\omega^2 + \gamma^2} \tag{17}$$

We know that at DC, $\omega = 0$ and considering only the real part of conductivity, we have simplified version of the conductivity known as DC conductivity as:

$$\sigma_{DC} = \frac{\varepsilon_0\omega_P^2}{\gamma} \tag{18}$$

Now, given by the experimental data, we extracted these parameters for three silicon samples using FIT@TDS software. We calculated the conductivity and hence resistivity ($1/\sigma_{DC}$) for all three Si wafer samples. These are tabulated below. Also, The Dc resistivity is measured using the Four-point probe methods (discuss later) to compare it with the calculated using FIT@TDS method. These are also shown in the table below.

Si wafer samples	Fitted Thickness	Fitted Plasma Frequency, ω_P (Hz)	Fitted decay Frequency, γ_P (Hz)	Fitted DC resistivity (or $1/\sigma_{DC}$) (Ohm-cm)	DC resistivity from Four-point probe (Ohm-cm)
520 µm Sample	505 µm	5.8×10^{12}	8.1×10^{12}	2.6	2.52±0.04
280 µm Sample	282 µm	2.3×10^{12}	8.1×10^{12}	17.6	16.59±0.63
290 µm Sample	284 µm	3.2×10^{12}	7.7×10^{12}	8.3	8.23±0.26

Table 4: Comparison of resistivity for three Si wafer samples using FIT@TDS method and Four-point probe method.

To verify my results using FIT@TDS method, I used another method to calculate resistivity of these samples. This method is one of the popular methods to calculate resistance for low resistivity sample. This is called Four-point probe method.

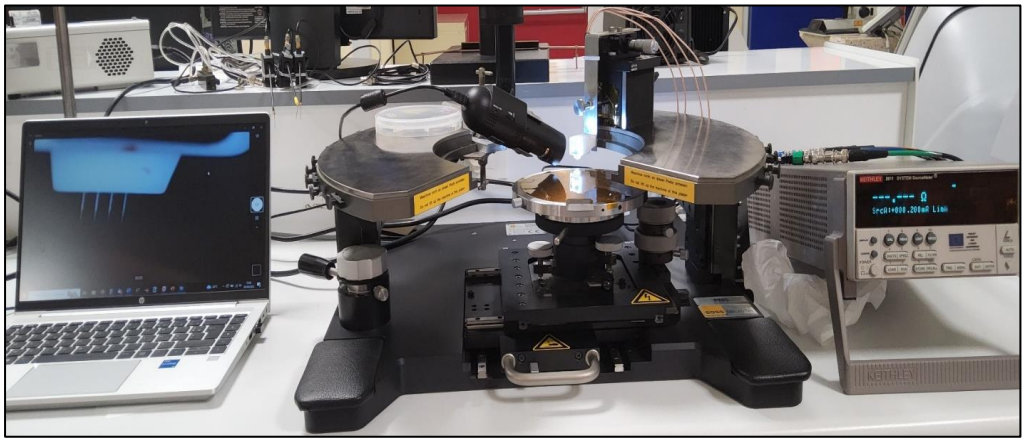

Fig 14: Four-point probe setup

The Four-point probe is a technique that measures resistivity of the sheet carrying charge carriers. It is a simple method that obeys Ohm's law. It contains four equally spaced probed that are made in contact with a material of thickness "t" and of unknown resistance. The current is forced from outer two probe and the resulting voltage is measured through two inner probes. The resistivity is given as:

$$\rho = \frac{\pi}{ln(2)} \times \left(\frac{V}{I}\right) \times t \times Correction\ value \qquad (19)$$

Here, t is thickness in cm, V is the voltage and I is the current. The correction value depends on the thickness of the sample. In our case, all samples were having thickness t≤0.5 mm, so the correction value is ≈ 0.96.

The resistivity calculated using this techniques are listed in Table 4 for better comparison.

2.5. Conclusion

In conclusion, we started with the characterisation of electronic parameters of three silicon wafer samples, each with different sizes, thickness and resistivity using FIT@TDS software. Then, we use this information to quantify the resistivity using Drude model. Finally, we also measured the resistivity of all the samples using Four-point probe technique. We compare these values evaluated from the two method and we can see a good agreement between the values of resistivity. Still, we didn't use the uncertainties on the resistivity evaluated using FIT@TDS method [10]. Also, in future the method can be tested for other novel samples with different resistivity.

3. Information Extraction from α-Lactose Samples Using THz-TDS

3.1. Sample preparation

The sample used for this experiment is α-Lactose monohydrate polycrystal powder purchased from Sigma-Aldrich, and used without any further purification. The lactose samples are considered as "Gold standard" in terahertz domain due to its easily observables absorption peaks at 0.53, 1.19 and 1.37 THz. Moreover, it is easily available and low cost makes it a good candidate for the start of the experiments. Although there are several points need to be taken into consideration. The pellets made out of the polycrystalline powder of lactose will possess slightly different optical properties than the single crystal. In case of single crystal, optical properties are highly anisotropic, which means that it will be dependent on crystallographic direction [20]. It makes the crystal to show strong birefringence. Whereas the polycrystalline pellet has random orientation of crystallite which makes it more isotropic and therefore it lacks birefringence.

The idea of this experiment is to get used to with the software and try another dispersive model other than Drude model which was used earlier for Silicon wafer. The sample is well grinded using mortar and pestle before making it into pellets to avoid inhomogeneity. Initially the sample were 100 percent lactose to study the behaviour of light matter interaction and get used to with FIT@TDS software [10]. The picture of the pellets is shown below.

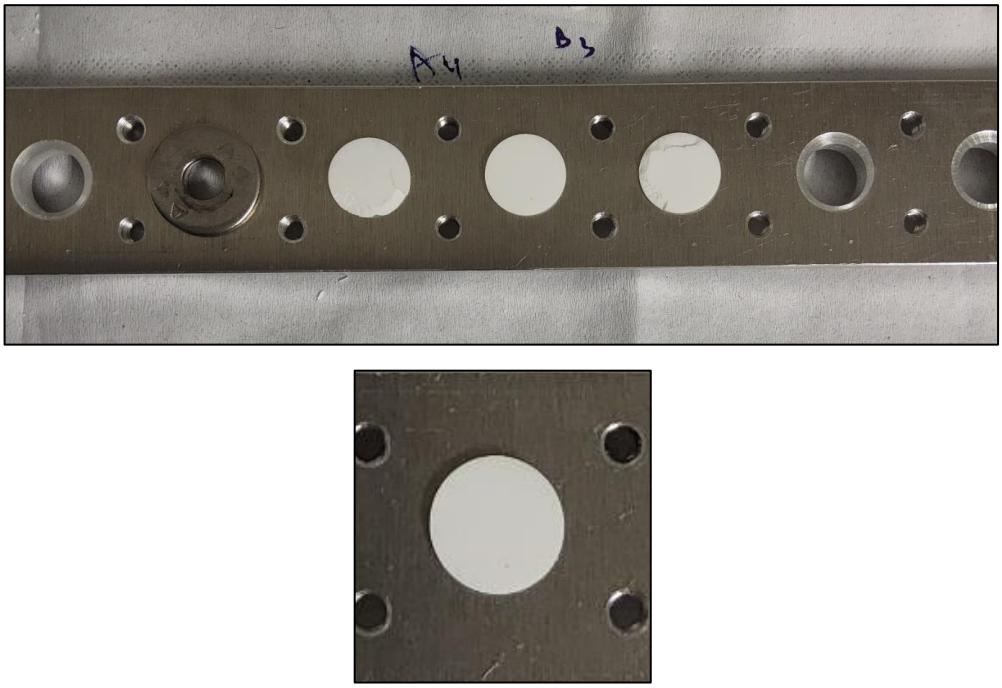

Fig 15: Lactose pellet sample with Aluminium stand.

3.2. Experimental methodology

Lactose show strong absorption peak at several THz frequencies. The peak resembles that of Lorentz profile. So, in this experiment, Lorentz model is used. Initially I started with the most significant peak at 0.53 THz then started adding other peaks. The spectra in time and frequency scale is shown in below figure.

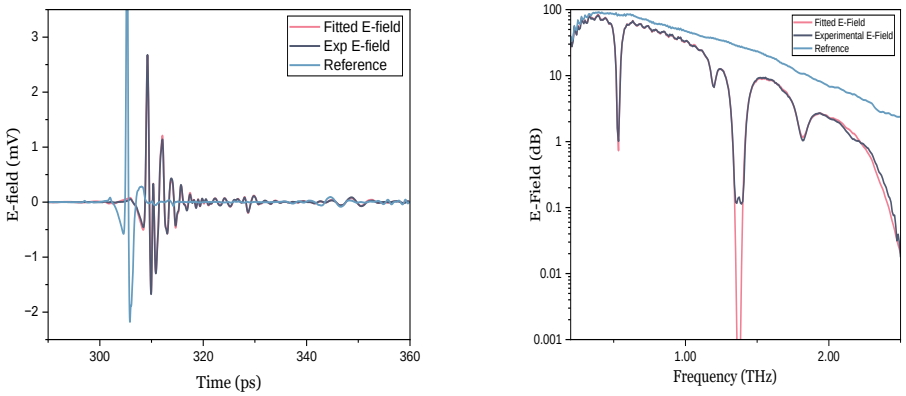

Fig 16: E-field in time and frequency scale.

The resulting real and imaginary part of refractive index are shown in another figure below.

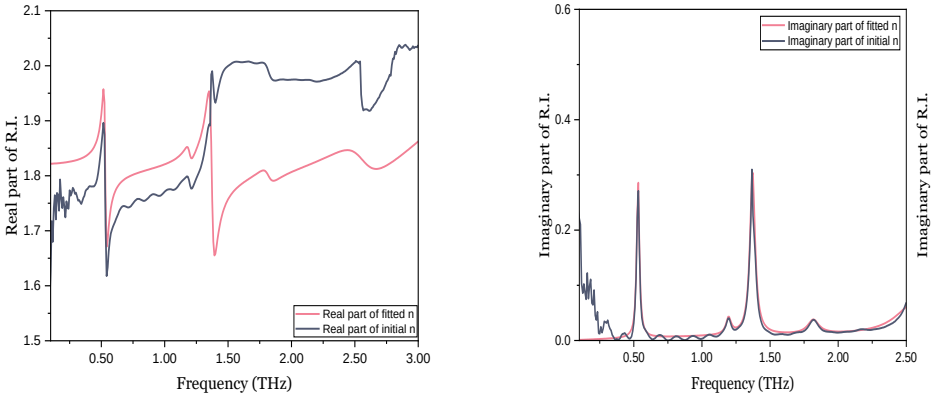

Fig 17: Real and imaginary part of fitted Refractive Index and its comparison with initial Refractive Index

Later, in this chapter an experimental methodology is discussed to use THz-TDS to quantify the concentration of the lactose in diluted sample.

3.3. Quantitative analysis of uncertainties on the refractive index of Lactose

In the scientific community, the data being extracted using any set of experimental tools has an important role to play. This is also true for the uncertainties in the data itself. Scientists have always shown keen interest in getting the better precision of their result,

whether it is from mathematical modelling or direct measurement from instruments. A lot of work is being done on daily basis to improve the variability of the instrument. Similarly, researchers are now putting efforts to estimate the uncertainties on the parameters extracted from mathematical modelling.

In this section, uncertainties on the optical parameters of the lactose sample are being estimated with the help of the Hessian matrix. The hessian matrix is a matrix that generates second order partial derivatives of a function. Mathematically, a function, f, with n variables which is written as,

$$f : R^n \rightarrow R \tag{16}$$

Then the Hessian matrix is given by:

$$H_f = \begin{bmatrix} \frac{\partial^2 f}{\partial x_1^2} & \cdots & \frac{\partial^2 f}{\partial x_1 x_n} \\ \vdots & \ddots & \vdots \\ \frac{\partial^2 f}{\partial x_n x_1} & \cdots & \frac{\partial^2 f}{\partial x_n^2} \end{bmatrix} \tag{17}$$

The Hessian matrix itself gives very important information about any function. It is used to determine the local extreme points of a function. In our case we started with two parameters, real part of refractive index (η) and imaginary part of the refractive index (κ). These will serves as the variable for our Error function, which is the modulus of residual error between measured and theoretically valued function. The error function is already optimised to get the best fit using various minimization techniques discuss earlier. This is done by our homemade software FIT@TDS to extract the optimised optical parameters from signal traces. Now, since the function is already optimised, the hessian matrix will show local minima when calculated at these optimised optical variables. This is more illustrated in figure below.

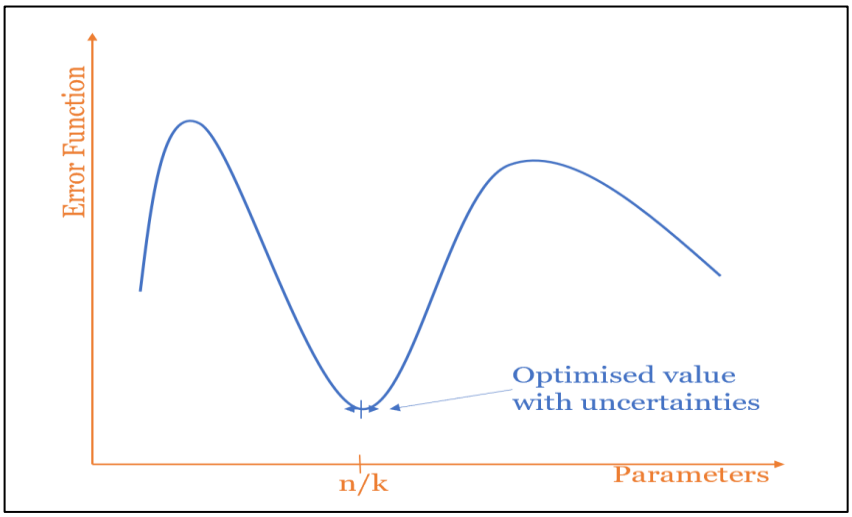

Fig 18: Optimised value of optical parameters from a given error function.

Since, we are interested in evaluating the uncertainties on our optical parameters, we are required to evaluate inverse of the Hessian matrix. The inverse of the Hessian matrix

of the likelihood function at an optimum point is estimated as the variance-covariance matrix of the parameters [21]. So, the standard deviation (or uncertainties) can be evaluated by taking diagonal elements of the inverse of the Hessian matrix. In order for uncertainties to have a physical significance, it should be normalised by the noise where signal is observed. The experimental errors have several sources in the TDS experiment such as delay line position drift, delay line speed variation, laser amplitude fluctuation and periodic sampling error [22].

So, to evaluate the Hessian Matrix and later error bars, we propose the usage of numerical derivation libraries supported by the python language. This is discussed in detail in the subsection of this section.

In the next section, the error bars on the complex absorption index for the lactose samples, through numerical hessian matrix calculations, are reported .

3.3.1. Standard deviation of transmission coefficient

For any optimization processes, the information about variability of signals is of utmost importance. It helps us to understand the uncertainties on the optimization parameters and quantitatively illustrate the effectiveness of optimization process. The standard deviation of the transmission coefficient reflects the valuable information about the variability of the data in the measurements. So, to estimate the uncertainties on our optical parameters through physical modelling, it is necessary to normalise it with the errors we are getting from measurements [23]. This is given by the summation of standard deviation of sample signal and reference signal multiplied with transfer function.

The complex transmission coefficient is defined as,

$$\tilde{T}(\omega) = \frac{\tilde{E}_S}{\tilde{E}_{ref}} \tag{18}$$

Here, $\tilde{E}_S$ and $\tilde{E}_{ref}$ are the Fourier transform of time domain THz signals $E_S(t)$ and $E_{ref}(t)$. Considering these variable as independent and errors corresponding to it is small as compared measured variable itself, the Taylor expansion of transmission coefficient is given by (neglecting higher order term):

$$d\tilde{T} = \frac{\partial \tilde{T}}{\partial \tilde{E}_S} d\tilde{E}_S + \frac{\partial \tilde{T}}{\partial \tilde{E}_{ref}} d\tilde{E}_{ref} \tag{19}$$

$$d\tilde{T} = \left[\frac{1}{\tilde{E}_{ref}} d\tilde{E}_S\right] + \left[-\frac{\tilde{E}_S}{\tilde{E}_{ref}^2} d\tilde{E}_{ref}\right] \tag{20}$$

In addition, variance for N points is defined as,

$$\tilde{\sigma}_T^2(\omega) = \frac{\sum_{i=1}^{N}(\tilde{T}_i - \tilde{T})^2}{N-1} = \frac{\sum_{i=1}^{N}(d\tilde{T}_i)^2}{N-1} \tag{21}$$

So,

$$\tilde{\sigma}_T^2(\omega) = \frac{1}{N-1}\left[\left(\frac{1}{\tilde{E}_{ref}^2}\right)\sum d\tilde{E}_S^2 + \left(\frac{\tilde{E}_S}{\tilde{E}_{ref}^2}\right)^2 \sum dE_{ref}^2\right] \quad (22)$$

And given that,

$$\frac{\sum_{i=1}^{N} d\tilde{E}_S{}^2}{N-1} = \tilde{\sigma}_{E_S}^2 \;\; And \;\; \frac{\sum_{i=1}^{N} d\tilde{E}_{ref}{}^2}{N-1} = \tilde{\sigma}_{E_{ref}}^2 \quad (23)$$

Here, $\tilde{\sigma}_{E_S}^2$ is the variance of sample signal and $\tilde{\sigma}_{E_{ref}}^2$ is the variance of reference signal. Putting equation (23) in (22) and taking square root to evaluate standard deviation,

$$\tilde{\sigma}_T(\omega) = \sqrt{\frac{1}{\tilde{E}_{ref}^2}\tilde{\sigma}_{E_S}^2 + \frac{\tilde{E}_S^2}{\tilde{E}_{ref}^4}\tilde{\sigma}_{E_{ref}}^2} \quad (24)$$

So, the inverse of hessian matrix of error function is normalized by the variance of the experimental data which is the summation of $\tilde{\sigma}_{E_S}^2$ and $\tilde{T}(\omega) * \tilde{\sigma}_{E_{ref}}^2$. The standard deviation of the measured reference and sample spectra can be retrieved through a home-written python script, soon to be publicly available.

3.3.2. Numerical method to evaluate uncertainties on optical parameters

The evaluation of the derivatives for the error function are very time consuming analytically, and keeping in mind the intention to extend the error estimation further than just the refractive index, and where the analytical derivation is not possible, it was necessary to imply numerical derivation methods to calculate the hessian matrix. There are several numerical methods like Finite difference method, Newton-Raphson method or Runge-Kutta method for the computation of second order partial derivation. In our case we are using the Python library Numdifftools. It is an excellent tool to solve numerical differentiation problems having one or more variables. It uses Finite differences method in adaptive manner so that user has the flexibility to choose complex-step, central, forward or backward finite differences. This tool is coupled with Richardson extrapolation methodology to maximize the accuracy of the result [24].

However, to make sure that the method is functioning properly in terms of derivation parameters, and the magnitude of our experimental values, the hessian calculation was also done analytically for comparison. From this we verified that there is a good agreement between Hessian matrix evaluated using Numdifftools and that calculated analytically using Sympy library in real field. An example of the hessian evaluation, as well as the comparison between the methods can be found in the Annex.

3.5. Quantification of lactose using THz-TDS

Since the development of Terahertz Time Domain Spectroscopy from last two decades, it shows rapid involvement in research communities not only for recording of the dielectric function [25] but also quantifying the constituents of the sample falling in the terahertz range. Several studies have shown that THz-TDS can be used to detect explosive substances, chemical recognition [25], detecting moisture content in the food [26] and detection of harmful residual out of honey sample down to the concentration of 1% by weight [27]. So, we procure the motivation to use this powerful technique to

quantify the concentration of the lactose in diluted sample. To do so, I prepared several samples with varying concentrations.

The use of THz-TDS for sensing applications seems to be very promising domain as we will show here. Although, this approach is of great interest for gas-phase studies, and it was initially planned for ammonia gas (detailed later in another chapter), we decided to test this approach for solid-phase, i.e., lactose. The basic idea is to develop a physical model that can extract the concentration of a sample, from the recorded spectra based on available spectroscopic data. Three parameters that are extracted for each Lorentz oscillator: $\Delta\varepsilon_k$, γ_k, ω_0 Knowing that concentration of the molecules is directly proportional to the line strength, $\Delta\varepsilon_k$. Therefore, including a concentration term as function of $\Delta\varepsilon_k$, we can extract the actual concentration of the sample, keeping all other parameters constant. I applied this idea on diluted lactose samples with varying concentrations. The lactose powder is diluted with polyethylene. Polyethylene is a thermoplastic material in polycrystalline form, which is almost transparent in Terahertz range. Below in table shows the different samples prepared with varying concentrations by adding Polyethylene.

S. No.	Concentration (in percentage w/w)	Mass of lactose (mg)	Mass of Polyethylene (mg)	Pressing weight (ton)
1.	100% ± 0.107%	131.7	0	5.10
2.	79.724% ± 0.097%	104.2	26.5	5.07
3.	59.607% ± 0.088%	78.8	53.4	5.02
4.	39.498% ± 0.082%	51.9	79.5	5.12
5.	20.713% ± 0.077%	27.3	104.5	5.02
6.	10.345% ± 0.077%	13.5	117.0	5.04
7.	3.191% ± 0.076%	4.2	127.4	5.12
8.	1.000% ± 0.077%	1.3	128.7	5.12
9.	0.296% ± 0.076%	0.39	131.3	5.12
10.	0%	0	131.6	5.02

Table 5: Various diluted lactose samples with their corresponding pressing pressure.

3.6. Results

This model fit fairly for Lactose sample. This can be seen in Fig 19. The absorption peak decreases as the concentration decreases. This shows that the model is following the proper trend.

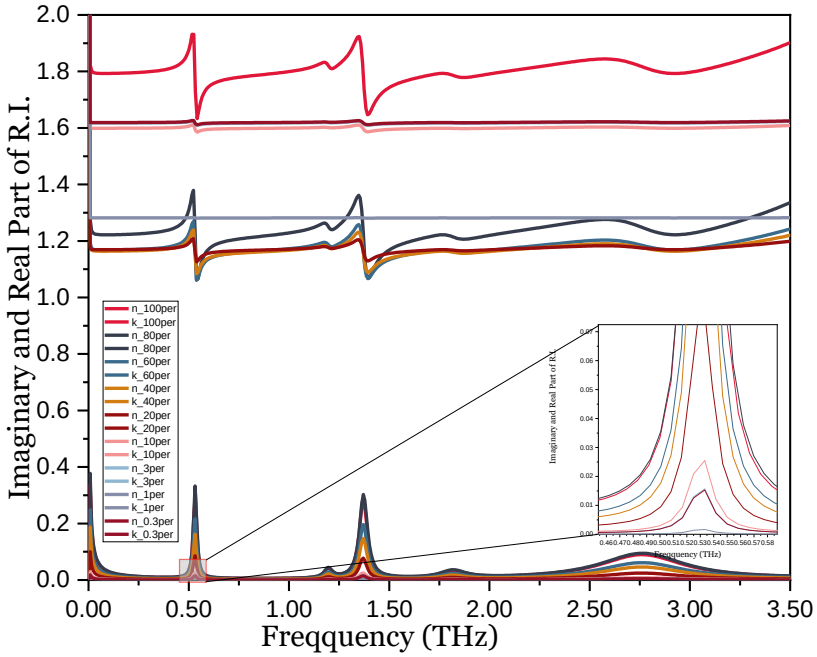

Fig 19: Real and imaginary part of refractive index for different diluted lactose samples.

Concentrations are simulated for all the diluted lactose samples prepared and then it is plotted with their corresponding actual concentration measured while preparing the sample (see Fig 19). The uncertainties on concentration while preparing the sample is also shown in the graph (Fig 20) through horizontal bars.

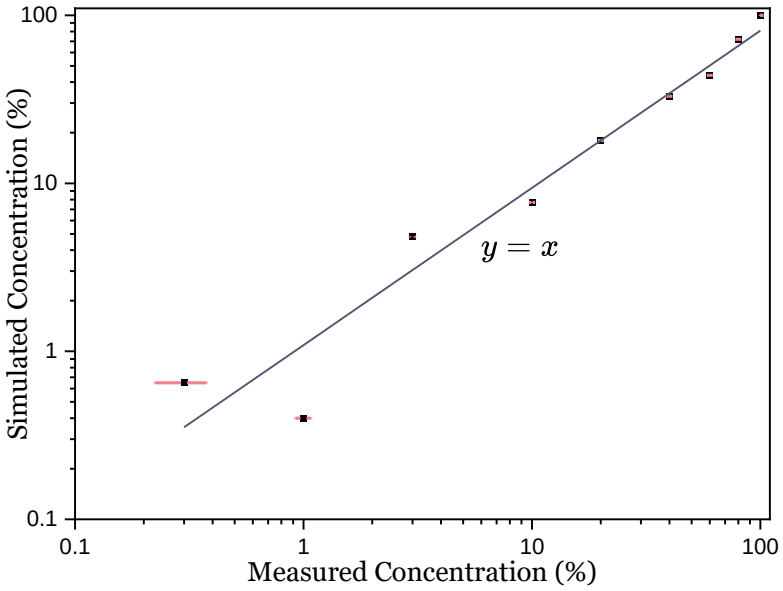

Fig 20: Illustration of simulated concentrations v/s actual concentrations.

From the above graph, we can see that the concentration matches fairly well at higher concentration but are not aligned at lower concentration. This is due to several reasons. One of the main reasons is that lactose samples are polycrystalline, which does not behave similarly to the single crystal. The lactose samples are denser and more complex than the gas molecules. The arrangement and structure of the lactose pellets can significantly affect how energy is transferred between the particles. In general, energy in solids can be transferred through lattice vibrations, defects, impurities and other mechanisms [28].

3.7. Conclusion

In conclusion, we started with fitting spectral traces of lactose sample using Lorentz model of dispersion in FIT@TDS to retrieve the complex refractive index of the sample. Then, we introduce a method that can estimate the standard deviation of the extracted parameters. This was done through Hessian matrix, evaluated numerically using library integrated within python programming language. Then the standard deviations were evaluated by taking square root of the inverse of the diagonal elements of this Hessian matrix. This has been shown graphically through error bars on optical parameters of lactose sample.

At the end, we have shown that the THZ-TDS could be used as a powerful technique to quantify the constituents of the sample showing fingerprints in terahertz region.

4. Sensitivity Measurement of THz-TDS for Gas molecules

4.1. Introduction

Gas spectroscopy or molecular spectroscopy is based on detection of molecular spectra (or atomic spectra) resulting from absorption or emission of electromagnetic radiation. These molecules undergo transition from one quantized energy level to other when interacting with the photons. Since the 19th century, several gas sensing techniques have been developed for example, semiconductor gas sensors, gas chromatography–mass spectrometry (GC–MS), infrared (IR) spectroscopy, and terahertz time-domain spectroscopy (THz-TDS) [29].

If we consider the electronic structure of molecules, it is well known that the difference in energies between the quantized rotational energy levels falls within the THz frequency domain. The pure vibrational modes however, are closer to the infrared region, yet some ro-vibrational states can be probed in the THz. Thus, we can say that the terahertz wave interacts with the gas sample, and when the frequency of the EM wave is resonant with the energy difference of two rotational levels, we observe absorption. [30].

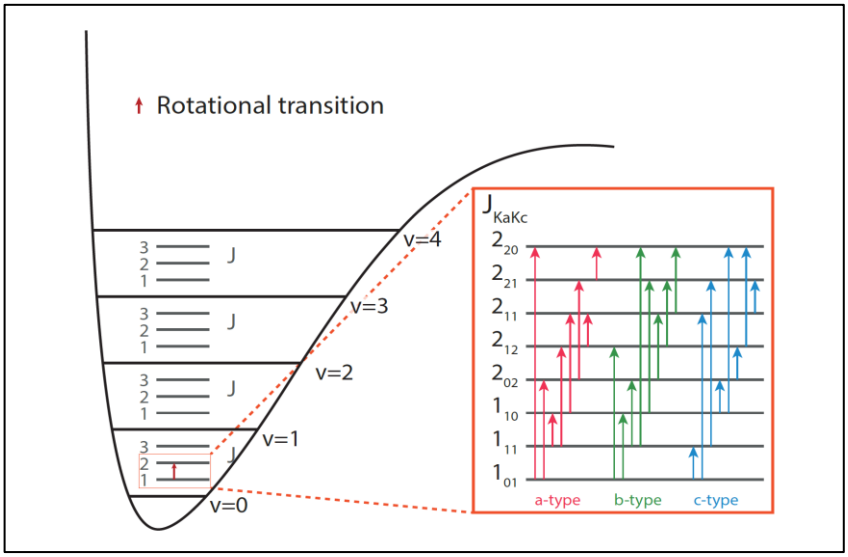

Fig 21: Illustration of transition of molecules based on selection rule for rotational and vibrational levels. This figure is taken from [31].

Line broadening plays a vital role in spectroscopy. Apart from natural broadening which is due to finite lifetime of the excited state of the molecules, there are other effects that cause line broadening like Doppler broadening and Pressure broadening. Doppler broadening is cause due to the distribution of velocities of atoms and molecules. Emitting (or absorbing) particles have different velocities causes different Doppler shift and the cumulative effect of which is the emission (or absorption) line broadening. Moreover, Pressure broadening is due to the collision of the molecules with other neighbouring atoms or molecules. It can be self-broadening due to collision with similar

molecules or more importantly, it can be air broadening caused by collision of alien molecules or atoms.

Using the Terahertz Time Domain Spectroscopic technique, spectrum parameters such as line strength $\Delta\mathcal{E}_k$, damping frequency γ_k, and oscillator frequency ω_0, are fitted to extract the spectroscopic parameters of the gas. In this work, I used these spectra parameters at a particular pressure as a reference to quantify the amount of gas molecules in a given experiment. This techniques can potentially be implemented for breathalyze. In the next section, it is described in more details.

4.2. Experimental setup

Terahertz Time Domain spectroscopy for gas sample is shown in figure below. It also consist of similar antennas as discussed in Si wafer experimental setup. The two antennas are placed inside two glass box purged with nitrogen gas. In this spectroscopy, THz radiation travels through a meter long tube interacting with the sample placed within it. Baratron is connected at the top of the tube to measure pressure inside the tube. The sample is injected through a small inlet shown in figure. This inlet is connected to an ammonia gas cylinder through a pipe. To vacuum out the sample tube, the tube is connected with vacuum pumps. In this experiment, we used three types of vacuum pumps. The primary pump which can vacuum the tube up to around 4 mbar. Then the primary pump is used in collaboration with the secondary pump that is capable of achieving a vacuum in microbars. Finally, an adsorption pump is also used when handling the harmful gas molecules. Adsorption pump consist of adsorption material like zeolite (Al_2O_3) which adsorb molecules inside the pores depending on the temperature.

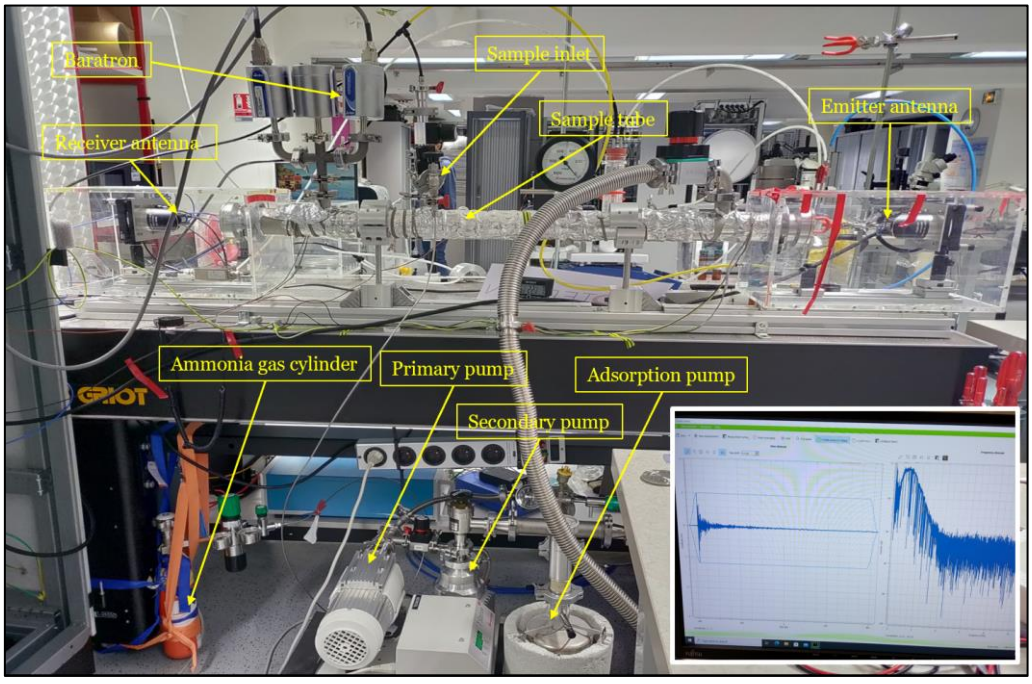

Fig 22: Experimental setup for gas sample measurement using THz-TDS. In the inlet, picture of spectrum traces in time and frequency domain.

4.3. Gas Model for sensitivity measurement

As we discussed earlier in page 7, the Lorentz model of permittivity is given as:

$$\tilde{\varepsilon} = \tilde{n}^2(\omega) = \tilde{\varepsilon}_\infty + \sum_{k=1}^{k_{max}} \frac{\Delta\varepsilon_k \omega_{0,k}^2}{\omega_{0,k}^2 - \omega^2 + j\omega\gamma_k} \tag{25}$$

We know that the spectrum line strength is proportional to partial pressure of the gas. So, given the reference line strength $\Delta\varepsilon_{k,ref}$, and reference partial pressure, P_{ref}, we can modify our model in such a way that we can extract the concentration of the gas at a given partial pressure. Herewith, defining our new line strength $\Delta\varepsilon'_k$ such that:

$$\Delta\varepsilon'_k = \boldsymbol{P_a} \frac{\Delta\varepsilon_{k,ref}}{P_{ref}} \tag{26}$$

Here, $\boldsymbol{P_a}$ is the partial pressure of gas (in our case ammonia molecules). Now, we just have one parameter as a variable to fit and we can evaluate the concentration of the gas. Using ideal gas law, Concentration, C of the gas is given by:

$$C = \frac{n}{V} = \frac{P_a}{RT} \tag{27}$$

This model is a preliminary work taking several assumptions in consideration. We assume that damping rate of radiation is independent of partial pressure and self-broadening is negligible at low partial pressure. Also, we are assuming that gas behaves ideally at the given pressure. Moreover, the experiments should be done at non-varying temperature and pressure.

A model taking into account the above assumptions and equations was implemented in FIT@TDS, and it permits to extract the experimental concentration from the recorded spectra based on well-known spectroscopic parameters.

In the next section, few simulations are shown at different partial pressure for Ammonia and their resultant concentration are illustrated on the graph.

4.4. Result and discussion

To demonstrate the working principle of the approach, we took the spectrum of 1000 ppm ammonia at 400 mbar as a reference to calculate the partial pressure. We have been given the spectroscopic parameters of ammonia at a total pressure of 400 mbar mixed with nitrogen molecules at room temperature. and I used it as reference file. The concentration of the ammonia was recorded as 1000 ppm. So, the partial pressure of the ammonia in this case is 0.4 mbar. The model was supplied with the total pressure at each experiment, and we managed to extract the partial pressures from the recorded spectra, and consequently to calculate the concentrations for the recorded spectra.

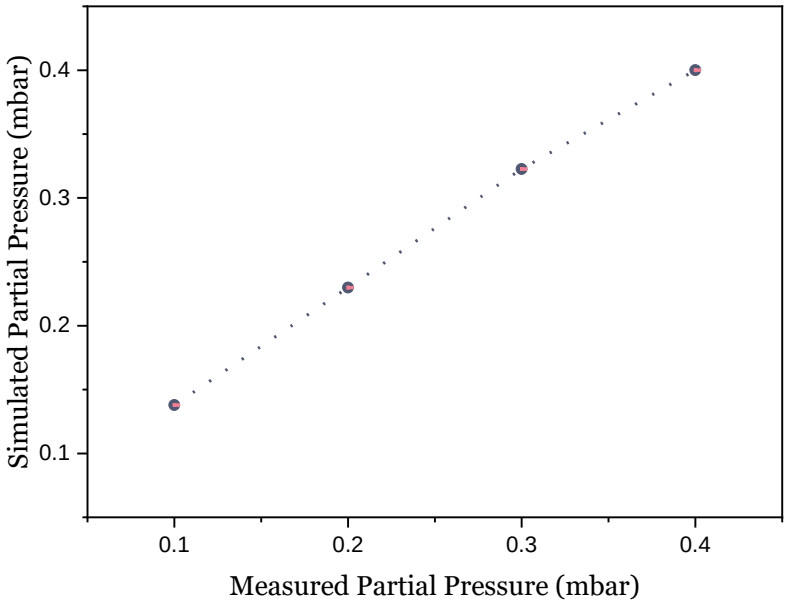

Fig 23: Graphical illustration of simulated partial pressure v/s measured partial pressure.

Again, the concentration of ammonia can be easily evaluated using equation no. 27. The above graph show that preliminary result to simulate and evaluate the amount of gas in the gas cell has good agreement with the actual measured value. Error bars on x-axis is show in pink in colour. This error is due to the instrumental error when measuring the pressure of the gas.

From this, we can say that this gas model can be implemented for further study and especially for breathalyser. Of course, this is a preliminary result and a simple model taken into consideration several assumptions. This can be improved by implementing more complex model that includes dependency of damping rate on pressure, behaviour of line strength at low and high pressure, etc. In fact, the idea of this model was to show that it possible to use THz-TDS spectrometer for a detection and quantification of trace gases, using an automated analysis routine, that make use of the available database data, or reference spectra recorded in the laboratory. The next step will be to record spectra diluted samples at atmospheric pressure and room temperature, with varying concentrations. The model then can be used to extract the concentrations from the recorded spectra using the proper assumptions.

4.5. Conclusion

From last few decades we have seen continuous developments in the field of gas sensing technique. Recently just after the growth of terahertz time domain spectroscopy, a more powerful technique for sensitivity measurement became the centre of attraction among the engineers and researchers. In this study, we demonstrated a new gas model which can be implemented along with dispersive model to estimate the concentration of the

gas. At the end, preliminary data is illustrated graphically for sensitivity measurement of ammonia that shows good agreement with theory discussed.

5. General Conclusion and Future Work

So, we started with the work on solving a scientific question for putting error bars (or uncertainties) on the extracted parameters from mathematical modelling and simulations. We proposed of using Hessian matrix on the function at optimised parameters. This inverse of this Hessian matrix will give the variance-covariance of the optimised parameters. Finally, taking square root of diagonal elements of the inverse of this matrix gives the uncertainties of the parameters of the function. This uncertainties if normalised with experimental error, is estimated as error on parameters, which has been extracted through mathematical modelling. We succeeded to calculate this error bars and will be demonstrated graphically on the optical parameters. Several other experiments has also been done using Terahertz Time Domain Spectroscopy to quantify the extracted parameters. Silicon wafer experiments were done to evaluate the resistivity of the semiconductor, similarly simulation experiments on ammonia gas has been done to quantify the sense the concentration of the gas. Whereas experiments on Lactose pellets were somehow more complex and shows insight for the improvements in the model.

This is for sure that there are a lot of improvements and future work to be done in this master's thesis. In the Silicon wafer section, there is a huge possibility that this can be used for other semiconductor samples at comparatively low charge carriers, only if we can validate the results at higher resistive samples. Lactose pellets are already a complex sample which need to be studied thoroughly taking into consideration of all the assumption made as a polycrystalline sample. The samples need to be prepared more systematically in order to work for measuring the sensitivity of the spectroscopy. Moreover, the gas model used in this work is a preliminary model and need further complexity. Overall, this work gives the direction to the researcher to quantitatively analyse the result. Interestingly, this is not limited only in the field of Terahertz, anyone who is working on mathematical modelling of a physical quantity can be benefitted by initial approach shown in this work.

Bibliography

[1] Andrew Fraknoi, David Morrison, and Sidney C. Wolff, *Astronomy*. Houston, Texas: OpenStax, 2016. [Online]. Available: https://openstax.org/books/astronomy/pages/1-introduction

[2] S. Reif-Acherman, 'Anders Jonas Ångström and the foundation of spectroscopy — Commemorative article on the second centenary of his birth', *Spectrochim. Acta Part B At. Spectrosc.*, vol. 102, pp. 12–23, Dec. 2014, doi: 10.1016/j.sab.2014.10.001.

[3] Simon Duckett and Bruce Gilbert, *Foundations of Spectroscopy Volume 78 of Oxford chemistry primers, ISSN 1367-109X Oxford science publications*. Oxford University Press, 2000.

[4] Melanie Lavancier, 'Melanie Lavancier. Heuristic approach to take up the challenge of terahertz time-domain spectroscopy for biology. Electronics. University of Lille, 2021. Français. ⟨NNT:2021LILUN008⟩ . ⟨tel-03539445⟩', University of Lille, 2022. [Online]. Available: https://theses.hal.science/tel-03539445

[5] T. Fortier and E. Baumann, '20 years of developments in optical frequency comb technology and applications', *Commun. Phys.*, vol. 2, no. 1, p. 153, Dec. 2019, doi: 10.1038/s42005-019-0249-y.

[6] N. Picqué and T. W. Hänsch, 'Frequency comb spectroscopy', *Nat. Photonics*, vol. 13, no. 3, pp. 146–157, Mar. 2019, doi: 10.1038/s41566-018-0347-5.

[7] B. Ferguson and X.-C. Zhang, 'Materials for terahertz science and technology', *Nat. Mater.*, vol. 1, no. 1, pp. 26–33, Sep. 2002, doi: 10.1038/nmat708.

[8] Y. Zhang, K. Li, and H. Zhao, 'Intense terahertz radiation: generation and application', *Front. Optoelectron.*, vol. 14, no. 1, pp. 4–36, Mar. 2021, doi: 10.1007/s12200-020-1052-9.

[9] P. Shumyatsky and R. R. Alfano, 'Terahertz sources', *J. Biomed. Opt.*, vol. 16, no. 3, p. 033001, 2011, doi: 10.1117/1.3554742.

[10] R. Peretti *et al.*, 'THz-TDS Time-Trace Analysis for the Extraction of Material and Metamaterial Parameters', *IEEE Trans. Terahertz Sci. Technol.*, vol. 9, no. 2, pp. 136–149, Mar. 2019, doi: 10.1109/TTHZ.2018.2889227.

[11] P. Drude, 'Zur Elektronentheorie der Metalle', *Ann. Phys.*, vol. 306, no. 3, pp. 566–613, 1900, doi: 10.1002/andp.19003060312.

[12] P. Drude, 'Zur Elektronentheorie der Metalle; II. Teil. Galvanomagnetische und thermomagnetische Effecte', *Ann. Phys.*, vol. 308, no. 11, pp. 369–402, 1900, doi: 10.1002/andp.19003081102.

[13] 'Drude model: Deriving the Conductivity and Permittivity of Metals', *Full Electrodynamics*. https://photonics101.com/light-matter-interactions/drude-model-metal-permittivity-conductivity

[14] S. Eliet, A. Cuisset, F. Hindle, J.-F. Lampin, and R. Peretti, 'Broadband Super-Resolution Terahertz Time-Domain Spectroscopy Applied to Gas Analysis', *IEEE Trans. Terahertz Sci. Technol.*, vol. 12, no. 1, pp. 75–80, Jan. 2022, doi: 10.1109/TTHZ.2021.3120029.

[15] C. Kim, J. S. Ahn, T. Ji, and J. B. Eom, 'Terahertz transmission properties of silicon wafers using continuous-wave terahertz spectroscopy', *Meas. Sci. Technol.*, vol. 28, no. 4, p. 045201, Apr. 2017, doi: 10.1088/1361-6501/aa57e5.

[16] E. Denakpo, T. Hannotte, M. Lavancier, S. E. Barois, and R. Peretti, 'Noise analysis, noise reduction and covariance estimation for Time domain Spectroscopy', in *2022 47th International Conference on Infrared, Millimeter and Terahertz Waves (IRMMW-THz)*, Delft, Netherlands: IEEE, Aug. 2022, pp. 1–2. doi: 10.1109/IRMMW-THz50927.2022.9895812.

[17] M. Lavancier *et al.*, 'Terahertz time domain spectroscopy data processing: analysing uncertainties to push boundaries', in *Terahertz Photonics II*, M. Jarrahi, D. Turchinovich, and S. Preu, Eds., Strasbourg, France: SPIE, May 2022, p. 9. doi: 10.1117/12.2620069.
[18] M. Lavancier, N. V. Yassine, J. Vlieghe, J.-F. Lampin, and R. Peretti, 'A criterion to compare permittivity models in the terahertz range', in *2021 46th International Conference on Infrared, Millimeter and Terahertz Waves (IRMMW-THz)*, Chengdu, China: IEEE, Aug. 2021, pp. 1–2. doi: 10.1109/IRMMW-THz50926.2021.9567242.
[19] F. S. Manciu, M. Manciu, W. G. Durrer, J. G. Salazar, K. H. Lee, and K. E. Bennet, 'A Drude model analysis of conductivity and free carriers in boron-doped diamond films and investigations of their internal stress and strain', *J. Mater. Sci.*, vol. 49, no. 16, pp. 5782–5789, Aug. 2014, doi: 10.1007/s10853-014-8309-x.
[20] M. I. Alonso, M. Garriga, N. Karl, J. O. Ossó, and F. Schreiber, 'Anisotropic optical properties of single crystalline PTCDA studied by spectroscopic ellipsometry', *Org. Electron.*, vol. 3, no. 1, pp. 23–31, Mar. 2002, doi: 10.1016/S1566-1199(01)00027-1.
[21] V. G. Dovì, O. Paladino, and A. P. Reverberi, 'Some remarks on the use of the inverse hessian matrix of the likelihood function in the estimation of statistical properties of parameters', *Appl. Math. Lett.*, vol. 4, no. 1, pp. 87–90, 1991, doi: 10.1016/0893-9659(91)90129-J.
[22] M. Naftaly, 'Metrology Issues and Solutions in THz Time-Domain Spectroscopy: Noise, Errors, Calibration', *IEEE Sens. J.*, vol. 13, no. 1, pp. 8–17, Jan. 2013, doi: 10.1109/JSEN.2012.2208624.
[23] M. Lavancier *et al.*, 'Terahertz time domain spectroscopy data processing: analysing uncertainties to push boundaries', in *Terahertz Photonics II*, M. Jarrahi, D. Turchinovich, and S. Preu, Eds., Strasbourg, France: SPIE, May 2022, p. 9. doi: 10.1117/12.2620069.
[24] Per A. Brodtkorb and John D'Errico, 'Numdifftools'. https://numdifftools.readthedocs.io/en/latest/intro/index.html
[25] B. Fischer, M. Hoffmann, H. Helm, G. Modjesch, and P. U. Jepsen, 'Chemical recognition in terahertz time-domain spectroscopy and imaging', *Semicond. Sci. Technol.*, vol. 20, no. 7, pp. S246–S253, Jul. 2005, doi: 10.1088/0268-1242/20/7/015.
[26] P. U. Jepsen, U. Møller, and H. Merbold, 'Investigation of aqueous alcohol and sugar solutions with reflection terahertz time-domain spectroscopy', *Opt. Express*, vol. 15, no. 22, p. 14717, 2007, doi: 10.1364/OE.15.014717.
[27] M. Massaouti, C. Daskalaki, A. Gorodetsky, A. D. Koulouklidis, and S. Tzortzakis, 'Detection of Harmful Residues in Honey Using Terahertz Time-Domain Spectroscopy', *Appl. Spectrosc.*, vol. 67, no. 11, pp. 1264–1269, Nov. 2013, doi: 10.1366/13-07111.
[28] '7. Spectra of Gases, Liquids, and Solids in the Far-Infrared', in *Methods in Experimental Physics*, Elsevier, 1973, pp. 302–441. doi: 10.1016/S0076-695X(08)60028-9.
[29] K. Komatsu, T. Iwamoto, H. Ito, and H. Saitoh, 'THz Gas Sensing Using Terahertz Time-Domain Spectroscopy with Ceramic Architecture', *ACS Omega*, vol. 7, no. 35, pp. 30768–30772, Sep. 2022, doi: 10.1021/acsomega.2c01635.
[30] F. C. D. Lucia, 'Spectroscopy in the Terahertz Spectral Region', in *Sensing with Terahertz Radiation*, D. Mittleman, Ed., in Springer Series in Optical Sciences, vol. 85. Berlin, Heidelberg: Springer Berlin Heidelberg, 2003, pp. 39–115. doi: 10.1007/978-3-540-45601-8_2.
[31] Noureddin Osseiran, 'Spectroscopic characterization of molecules of atmospheric interest: Internal dynamics and microsolvation with hydrogen sulfide (H2S)', University of Lille. [Online]. Available: https://www.theses.fr/en/2021LILUR062

Annex

Analytical method to evaluate uncertainties on optical parameters

In this section, the important question needs to be addressed that how we can evaluate analytically the uncertainties for the complex transmission coefficient for an air medium normal interface which is given by:

$$\tilde{T}(\omega) = \frac{4\tilde{n}}{(\tilde{n}+1)^2} \times Exp\left(-j\frac{\omega d}{c}(\tilde{n}-1)\right) \tag{28}$$

Here, $\tilde{n}$ is the refractive index, ω is the angular frequency of the EM wave, d is the thickness of the sample, c is the speed of light in vacuum. For simplicity, we have not taken into account the Fabry-Perot term here.

In fitting process, an error function is defined for any physical model and is given by the squared modulus of difference between measured and theoretical valued function.

$$Error_f = |MeasZ - TheoZ|^2 \tag{29}$$

Assuming, $MeasZ = y$ for derivation

$$Error_f = \left|\tilde{y} - \frac{4\tilde{n}}{(\tilde{n}+1)^2} Exp\left(-j\frac{\omega d}{c}(\tilde{n}-1)\right)\right|^2 \tag{30}$$

$$Error_{\tilde{f}} = \left[\tilde{y} - \frac{4\tilde{n}}{(\tilde{n}+1)^2} Exp\left(-j\frac{\omega d}{c}(\tilde{n}-1)\right)\right]\left[\tilde{y} - \frac{4\tilde{n}}{(\tilde{n}+1)^2} Exp\left(-j\frac{\omega d}{c}(\tilde{n}-1)\right)\right]^* \tag{31}$$

To calculate the uncertainties on the optical parameters (in our case, real part 'η' and imaginary part 'κ' of refractive index 'n'), we are required to evaluate the Hessian for the error function. But, to solve second derivative of error function in complex field was the constraint. I simplified the equation manually and retrieved the error function in real field. In deriving the equation we have the following variables,

Refractive index,

$$\tilde{n} = \tilde{\eta} + i\tilde{\kappa} \tag{32}$$

And assuming $\tilde{y}$ as a complex variable,

$$\tilde{y} = \tilde{c}_1 + i\tilde{c}_2 \tag{33}$$

So, the error function is derived as,

$$Error_{\tilde{f}} = \tilde{c}_1^2 + \tilde{c}_2^2 - 2\left(\tilde{c}_1\tilde{a}_1 - \tilde{c}_2\tilde{b}_1\right)Exp\left(-\tilde{d}_1\right)Cos\left(\tilde{d}_2\right) + 2\left(\tilde{c}_1\tilde{b}_1 + \tilde{a}_1\tilde{c}_2\right)Exp\left(-\tilde{d}_1\right)Sin\left(\tilde{d}_2\right) + \tilde{a}_1^2 Exp\left(-2\tilde{d}_1\right) + \tilde{b}_1^2 Exp\left(-2\tilde{d}_1\right) \tag{34}$$

Given that,

$$\tilde{d}_1 = \frac{\omega d\tilde{\kappa}}{c} \tag{35}$$

$$\tilde{d}_2 = \frac{\omega d}{c}(\tilde{\eta} - 1) \tag{36}$$

$$\tilde{a}_1 = \frac{4\tilde{\eta}^3 + 4\tilde{\eta}.\tilde{\kappa}^2 + 8\tilde{\eta}^2 + 8\tilde{\kappa}^2 + 4\tilde{\eta}}{(\tilde{\kappa}^2 + (1+\tilde{\eta})^2)^2} \tag{37}$$

$$\tilde{b}_1 = \frac{4\tilde{\kappa}(1 - \tilde{\eta}^2 - \tilde{\kappa}^2)}{(\tilde{\kappa}^2 + (1+\tilde{\eta})^2)^2} \tag{38}$$

For the first step, our goal is to evaluate error bars or uncertainties on the $\tilde{\eta}$ and $\tilde{\kappa}$ of the transmission coefficient model mentioned above.

Initially we verify our derivation. To do so we solve for $\tilde{y}$ such that the Error function is zero and evaluated the first order differentiation of error function at this $\tilde{y}$.

$$\left[\tilde{y} - \frac{4\tilde{n}}{(\tilde{n}+1)^2} Exp\left(-j\frac{\omega d}{c}(\tilde{n}-1)\right)\right] = 0 \tag{39}$$

Since this is the minimum value of the Error function, the First order derivatives at this point should be zero. Then the Hessian is evaluated which is the second order partial derivative of the function. The Hessian matrix is calculated using the Mathematica tool and verified by using Sympy module. Sympy is a Python library for symbolic expression and calculation. All the elements of Hessian matrix, H_{11}, H_{12}, H_{21}, and H_{22} can be found in Annexure I.

For an example, I took one of the values from Silicon sample at the frequency of 1002673839688.8643 Hz to be $\tilde{\eta}$ = 4.225008509053177 and $\tilde{\kappa}$ = 0.05738368802648747. The value of $\tilde{y}$ comes out to be 0.438553-0.0520706i. The Hessian matrix calculated using this parameters knowing other values like thickness and speed of light, c is

$$\begin{pmatrix} 19.2136 & 1.04777\times10^{-15} \\ 1.04777\times10^{-15} & 19.2136 \end{pmatrix}$$

I then, evaluated the Hessian matrix putting the value of MeasZ from the data extracted from experiment. In this way we can get the idea of actual uncertainties in real field. Here is the updated Hessian matrix.

$$\begin{pmatrix} 19.2132 & -0.00880367 \\ -0.00880367 & 19.214 \end{pmatrix}$$

The code and the result shown below to evaluate Hessian matrix in complex field using Numdifftools.

```
import numpy as np
import numdifftools as nd

w = 2*np.pi*1002673839688.8643
d = 0.000280
c = 299792458
y = 0.5265556348864405

z = lambda x: x[0]-1j*x[1]

f = lambda x: abs((y-((4*z(x)/((z(x) + 1)**2))*np.exp(
    -1j*w*d/c*(z(x) - 1))))**2)

H = nd.Hessian(f)([4.204274308768241, 0.028012991437861 75])

print("Hessian matrix:")
print(H)
```

```
Hessian matrix:
[[ 1.92132561e+01 -9.10926218e-03]
 [-9.10926218e-03  1.92140524e+01]]
```

Fig 24: Screenshot of the python code to evaluate Hessian matrix and its result.

Later it is compared using Numdifftools in Real field and using analytical method like Sympy library in python in Real field. Below is the output to show all three at one place for better comparison.

```
Hessian using Numdiff in C :  [[ 1.92128254e+01 -7.99162694e-06]
 [-7.99162694e-06  1.92128697e+01]]
Hessian using Numdiff in R :  [[ 1.92128254e+01 -7.99162149e-06]
 [-7.99162149e-06  1.92128697e+01]]
Hessian using sympy in R :  Matrix([[19.2128253540913, -7.99162695317073e-6], [-7.99162695317073e-6, 19.2128697245116]])
```

Fig 25: Screenshot of the result of the Hessian matrix using numerical and analytical method in complex and real field.

From this, we can see that there is a good agreement between Hessian matrix evaluated using Numdifftools in complex field and also in real field. This is also compared and found good agreement with the Hessian matrix calculated analytically using Sympy library in real field.

1. Hessian Matrix, H_{11}, calculated using Mathematica software

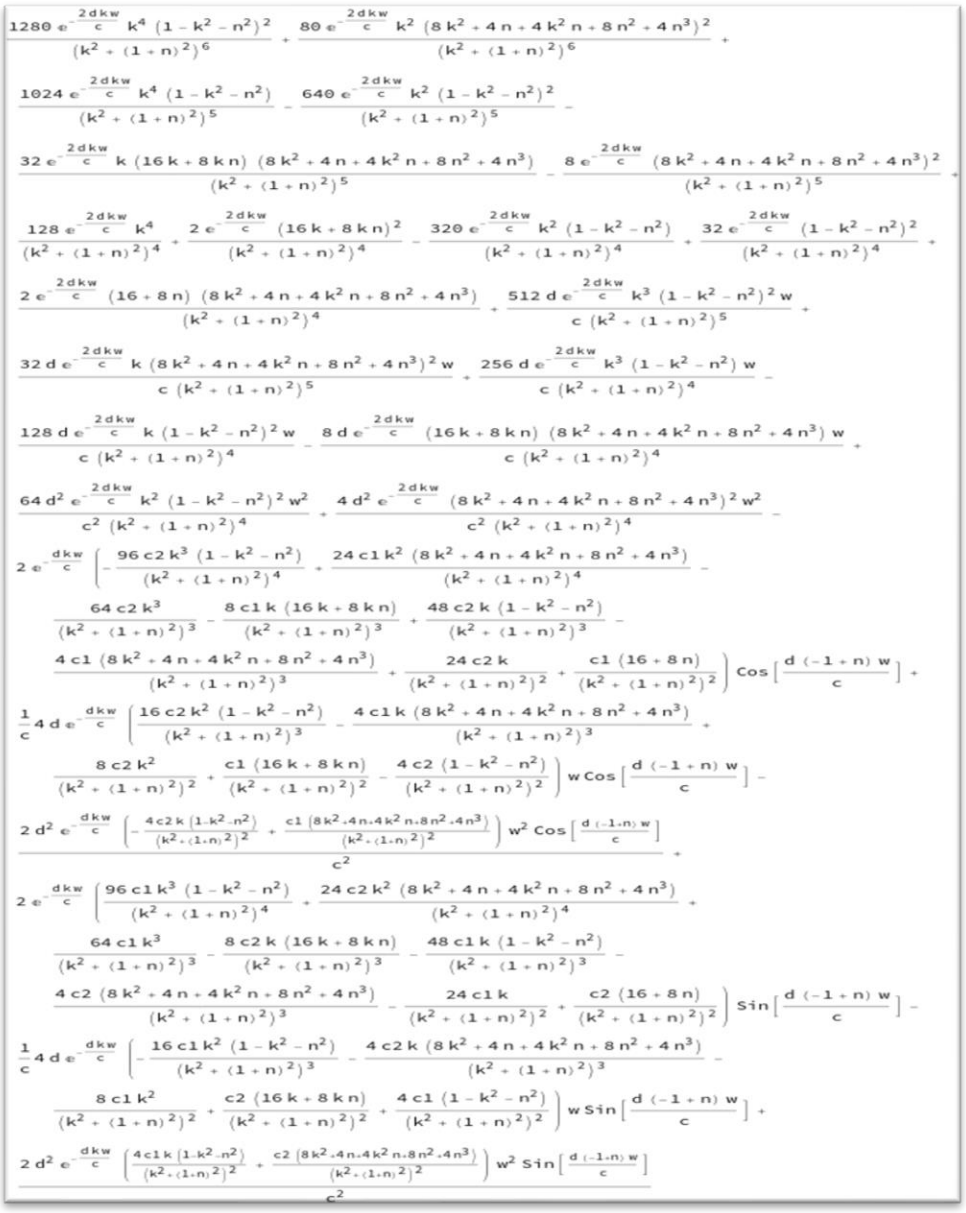

$$\frac{1280\, e^{-\frac{2dkw}{c}} k^4 (1-k^2-n^2)^2}{(k^2+(1+n)^2)^6} + \frac{80\, e^{-\frac{2dkw}{c}} k^2 (8k^2+4n+4k^2n+8n^2+4n^3)^2}{(k^2+(1+n)^2)^6} +$$

$$\frac{1024\, e^{-\frac{2dkw}{c}} k^4 (1-k^2-n^2)}{(k^2+(1+n)^2)^5} - \frac{640\, e^{-\frac{2dkw}{c}} k^2 (1-k^2-n^2)^2}{(k^2+(1+n)^2)^5} -$$

$$\frac{32\, e^{-\frac{2dkw}{c}} k (16k+8kn)(8k^2+4n+4k^2n+8n^2+4n^3)}{(k^2+(1+n)^2)^5} - \frac{8\, e^{-\frac{2dkw}{c}} (8k^2+4n+4k^2n+8n^2+4n^3)^2}{(k^2+(1+n)^2)^5} +$$

$$\frac{128\, e^{-\frac{2dkw}{c}} k^4}{(k^2+(1+n)^2)^4} + \frac{2\, e^{-\frac{2dkw}{c}} (16k+8kn)^2}{(k^2+(1+n)^2)^4} - \frac{320\, e^{-\frac{2dkw}{c}} k^2 (1-k^2-n^2)}{(k^2+(1+n)^2)^4} + \frac{32\, e^{-\frac{2dkw}{c}} (1-k^2-n^2)^2}{(k^2+(1+n)^2)^4} +$$

$$\frac{2\, e^{-\frac{2dkw}{c}} (16+8n)(8k^2+4n+4k^2n+8n^2+4n^3)}{(k^2+(1+n)^2)^4} + \frac{512\, d\, e^{-\frac{2dkw}{c}} k^3 (1-k^2-n^2)^2 w}{c\,(k^2+(1+n)^2)^5} +$$

$$\frac{32\, d\, e^{-\frac{2dkw}{c}} k (8k^2+4n+4k^2n+8n^2+4n^3)^2 w}{c\,(k^2+(1+n)^2)^5} + \frac{256\, d\, e^{-\frac{2dkw}{c}} k^3 (1-k^2-n^2) w}{c\,(k^2+(1+n)^2)^4} -$$

$$\frac{128\, d\, e^{-\frac{2dkw}{c}} k (1-k^2-n^2)^2 w}{c\,(k^2+(1+n)^2)^4} - \frac{8\, d\, e^{-\frac{2dkw}{c}} (16k+8kn)(8k^2+4n+4k^2n+8n^2+4n^3) w}{c\,(k^2+(1+n)^2)^4} +$$

$$\frac{64\, d^2\, e^{-\frac{2dkw}{c}} k^2 (1-k^2-n^2)^2 w^2}{c^2 (k^2+(1+n)^2)^4} + \frac{4\, d^2\, e^{-\frac{2dkw}{c}} (8k^2+4n+4k^2n+8n^2+4n^3)^2 w^2}{c^2 (k^2+(1+n)^2)^4} -$$

$$2\, e^{-\frac{dkw}{c}} \left(-\frac{96\, c2\, k^3 (1-k^2-n^2)}{(k^2+(1+n)^2)^4} + \frac{24\, c1\, k^2 (8k^2+4n+4k^2n+8n^2+4n^3)}{(k^2+(1+n)^2)^4} - \right.$$

$$\frac{64\, c2\, k^3}{(k^2+(1+n)^2)^3} - \frac{8\, c1\, k (16k+8kn)}{(k^2+(1+n)^2)^3} + \frac{48\, c2\, k (1-k^2-n^2)}{(k^2+(1+n)^2)^3} -$$

$$\left. \frac{4\, c1 (8k^2+4n+4k^2n+8n^2+4n^3)}{(k^2+(1+n)^2)^3} + \frac{24\, c2\, k}{(k^2+(1+n)^2)^2} + \frac{c1 (16+8n)}{(k^2+(1+n)^2)^2} \right) \mathrm{Cos}\left[\frac{d(-1+n)w}{c}\right] +$$

$$\frac{1}{c} 4\, d\, e^{-\frac{dkw}{c}} \left(\frac{16\, c2\, k^2 (1-k^2-n^2)}{(k^2+(1+n)^2)^3} - \frac{4\, c1\, k (8k^2+4n+4k^2n+8n^2+4n^3)}{(k^2+(1+n)^2)^3} + \right.$$

$$\left. \frac{8\, c2\, k^2}{(k^2+(1+n)^2)^2} + \frac{c1 (16+8n)}{(k^2+(1+n)^2)^2} - \frac{4\, c2 (1-k^2-n^2)}{(k^2+(1+n)^2)^2} \right) w \mathrm{Cos}\left[\frac{d(-1+n)w}{c}\right] -$$

$$\frac{2\, d^2\, e^{-\frac{dkw}{c}} \left(-\frac{4\, c2\, k (1-k^2-n^2)}{(k^2+(1+n)^2)^2} + \frac{c1 (8k^2+4n+4k^2n+8n^2+4n^3)}{(k^2+(1+n)^2)^2} \right) w^2 \mathrm{Cos}\left[\frac{d(-1+n)w}{c}\right]}{c^2} +$$

$$2\, e^{-\frac{dkw}{c}} \left(\frac{96\, c1\, k^3 (1-k^2-n^2)}{(k^2+(1+n)^2)^4} + \frac{24\, c2\, k^2 (8k^2+4n+4k^2n+8n^2+4n^3)}{(k^2+(1+n)^2)^4} + \right.$$

$$\frac{64\, c1\, k^3}{(k^2+(1+n)^2)^3} - \frac{8\, c2\, k (16k+8kn)}{(k^2+(1+n)^2)^3} - \frac{48\, c1\, k (1-k^2-n^2)}{(k^2+(1+n)^2)^3} -$$

$$\left. \frac{4\, c2 (8k^2+4n+4k^2n+8n^2+4n^3)}{(k^2+(1+n)^2)^3} - \frac{24\, c1\, k}{(k^2+(1+n)^2)^2} + \frac{c2 (16+8n)}{(k^2+(1+n)^2)^2} \right) \mathrm{Sin}\left[\frac{d(-1+n)w}{c}\right] -$$

$$\frac{1}{c} 4\, d\, e^{-\frac{dkw}{c}} \left(-\frac{16\, c1\, k^2 (1-k^2-n^2)}{(k^2+(1+n)^2)^3} - \frac{4\, c2\, k (8k^2+4n+4k^2n+8n^2+4n^3)}{(k^2+(1+n)^2)^3} - \right.$$

$$\left. \frac{8\, c1\, k^2}{(k^2+(1+n)^2)^2} + \frac{c2 (16+8n)}{(k^2+(1+n)^2)^2} + \frac{4\, c1 (1-k^2-n^2)}{(k^2+(1+n)^2)^2} \right) w \mathrm{Sin}\left[\frac{d(-1+n)w}{c}\right] +$$

$$\frac{2\, d^2\, e^{-\frac{dkw}{c}} \left(\frac{4\, c1\, k (1-k^2-n^2)}{(k^2+(1+n)^2)^2} + \frac{c2 (8k^2+4n+4k^2n+8n^2+4n^3)}{(k^2+(1+n)^2)^2} \right) w^2 \mathrm{Sin}\left[\frac{d(-1+n)w}{c}\right]}{c^2}$$

2. Hessian Matrix, $H_{12}=H_{21}$

$$\frac{1280\, e^{-\frac{2dkw}{c}} k^3 (1+n) (1-k^2-n^2)^2}{(k^2+(1+n)^2)^6} + \frac{80\, e^{-\frac{2dkw}{c}} k (1+n) (8k^2+4n+4k^2n+8n^2+4n^3)^2}{(k^2+(1+n)^2)^6} +$$

$$\frac{512\, e^{-\frac{2dkw}{c}} k^3 n (1-k^2-n^2)}{(k^2+(1+n)^2)^5} + \frac{512\, e^{-\frac{2dkw}{c}} k^3 (1+n) (1-k^2-n^2)}{(k^2+(1+n)^2)^5} -$$

$$\frac{256\, e^{-\frac{2dkw}{c}} k (1+n) (1-k^2-n^2)^2}{(k^2+(1+n)^2)^5} - \frac{16\, e^{-\frac{2dkw}{c}} (1+n) (16k+8kn) (8k^2+4n+4k^2n+8n^2+4n^3)}{(k^2+(1+n)^2)^5}$$

$$\frac{16\, e^{-\frac{2dkw}{c}} k (4+4k^2+16n+12n^2) (8k^2+4n+4k^2n+8n^2+4n^3)}{(k^2+(1+n)^2)^5} + \frac{128\, e^{-\frac{2dkw}{c}} k^3 n}{(k^2+(1+n)^2)^4} -$$

$$\frac{128\, e^{-\frac{2dkw}{c}} kn (1-k^2-n^2)}{(k^2+(1+n)^2)^4} + \frac{2\, e^{-\frac{2dkw}{c}} (16k+8kn) (4+4k^2+16n+12n^2)}{(k^2+(1+n)^2)^4} +$$

$$\frac{16\, e^{-\frac{2dkw}{c}} k (8k^2+4n+4k^2n+8n^2+4n^3)}{(k^2+(1+n)^2)^4} + \frac{256\, d\, e^{-\frac{2dkw}{c}} k^2 (1+n) (1-k^2-n^2)^2 w}{c (k^2+(1+n)^2)^5} +$$

$$\frac{16\, d\, e^{-\frac{2dkw}{c}} (1+n) (8k^2+4n+4k^2n+8n^2+4n^3)^2 w}{c (k^2+(1+n)^2)^5} + \frac{128\, d\, e^{-\frac{2dkw}{c}} k^2 n (1-k^2-n^2) w}{c (k^2+(1+n)^2)^4} -$$

$$\frac{4\, d\, e^{-\frac{2dkw}{c}} (4+4k^2+16n+12n^2) (8k^2+4n+4k^2n+8n^2+4n^3) w}{c (k^2+(1+n)^2)^4} -$$

$$2\, e^{-\frac{dkw}{c}} \left(-\frac{96\, c2\, k^2 (1+n) (1-k^2-n^2)}{(k^2+(1+n)^2)^4} + \frac{24\, c1\, k (1+n) (8k^2+4n+4k^2n+8n^2+4n^3)}{(k^2+(1+n)^2)^4} - \right.$$

$$\frac{32\, c2\, k^2 n}{(k^2+(1+n)^2)^3} - \frac{32\, c2\, k^2 (1+n)}{(k^2+(1+n)^2)^3} - \frac{4\, c1\, (1+n) (16k+8kn)}{(k^2+(1+n)^2)^3} + \frac{16\, c2\, (1+n) (1-k^2-n^2)}{(k^2+(1+n)^2)^3} -$$

$$\left. \frac{4\, c1\, k (4+4k^2+16n+12n^2)}{(k^2+(1+n)^2)^3} + \frac{8\, c1\, k}{(k^2+(1+n)^2)^2} + \frac{8\, c2\, n}{(k^2+(1+n)^2)^2} \right) \mathrm{Cos}\left[\frac{d(-1+n)w}{c}\right] +$$

$$\frac{1}{c} 2\, d\, e^{-\frac{dkw}{c}} \left(-\frac{16\, c1\, k^2 (1-k^2-n^2)}{(k^2+(1+n)^2)^3} - \frac{4\, c2\, k (8k^2+4n+4k^2n+8n^2+4n^3)}{(k^2+(1+n)^2)^3} - \right.$$

$$\left. \frac{8\, c1\, k^2}{(k^2+(1+n)^2)^2} + \frac{c2\, (16k+8kn)}{(k^2+(1+n)^2)^2} + \frac{4\, c1\, (1-k^2-n^2)}{(k^2+(1+n)^2)^2} \right) w \mathrm{Cos}\left[\frac{d(-1+n)w}{c}\right] + \frac{1}{c}$$

$$2\, d\, e^{-\frac{dkw}{c}} \left(\frac{16\, c2\, k (1+n) (1-k^2-n^2)}{(k^2+(1+n)^2)^3} - \frac{4\, c1\, (1+n) (8k^2+4n+4k^2n+8n^2+4n^3)}{(k^2+(1+n)^2)^3} + \right.$$

$$\left. \frac{8\, c2\, kn}{(k^2+(1+n)^2)^2} + \frac{c1\, (4+4k^2+16n+12n^2)}{(k^2+(1+n)^2)^2} \right) w \mathrm{Cos}\left[\frac{d(-1+n)w}{c}\right] -$$

$$\frac{2\, d^2\, e^{-\frac{dkw}{c}} \left(\frac{4\, c1\, k (1-k^2-n^2)}{(k^2+(1+n)^2)^2} + \frac{c2\, (8k^2+4n+4k^2n+8n^2+4n^3)}{(k^2+(1+n)^2)^2} \right) w^2 \mathrm{Cos}\left[\frac{d(-1+n)w}{c}\right]}{c^2} +$$

$$2\, e^{-\frac{dkw}{c}} \left(\frac{96\, c1\, k^2 (1+n) (1-k^2-n^2)}{(k^2+(1+n)^2)^4} + \frac{24\, c2\, k (1+n) (8k^2+4n+4k^2n+8n^2+4n^3)}{(k^2+(1+n)^2)^4} + \right.$$

$$\frac{32\, c1\, k^2 n}{(k^2+(1+n)^2)^3} + \frac{32\, c1\, k^2 (1+n)}{(k^2+(1+n)^2)^3} - \frac{4\, c2\, (1+n) (16k+8kn)}{(k^2+(1+n)^2)^3} - \frac{16\, c1\, (1+n) (1-k^2-n^2)}{(k^2+(1+n)^2)^3} -$$

$$\left. \frac{4\, c2\, k (4+4k^2+16n+12n^2)}{(k^2+(1+n)^2)^3} + \frac{8\, c2\, k}{(k^2+(1+n)^2)^2} - \frac{8\, c1\, n}{(k^2+(1+n)^2)^2} \right) \mathrm{Sin}\left[\frac{d(-1+n)w}{c}\right] +$$

$$\frac{1}{c} 2\, d\, e^{-\frac{dkw}{c}} \left(\frac{16\, c2\, k^2 (1-k^2-n^2)}{(k^2+(1+n)^2)^3} - \frac{4\, c1\, k (8k^2+4n+4k^2n+8n^2+4n^3)}{(k^2+(1+n)^2)^3} + \right.$$

$$\left. \frac{8\, c2\, k^2}{(k^2+(1+n)^2)^2} + \frac{c1\, (16k+8kn)}{(k^2+(1+n)^2)^2} - \frac{4\, c2\, (1-k^2-n^2)}{(k^2+(1+n)^2)^2} \right) w \mathrm{Sin}\left[\frac{d(-1+n)w}{c}\right] - \frac{1}{c}$$

$$2\, d\, e^{-\frac{dkw}{c}} \left(-\frac{16\, c1\, k (1+n) (1-k^2-n^2)}{(k^2+(1+n)^2)^3} - \frac{4\, c2\, (1+n) (8k^2+4n+4k^2n+8n^2+4n^3)}{(k^2+(1+n)^2)^3} - \right.$$

$$\left. \frac{8\, c1\, kn}{(k^2+(1+n)^2)^2} + \frac{c2\, (4+4k^2+16n+12n^2)}{(k^2+(1+n)^2)^2} \right) w \mathrm{Sin}\left[\frac{d(-1+n)w}{c}\right] -$$

$$\frac{2\, d^2\, e^{-\frac{dkw}{c}} \left(-\frac{4\, c2\, k (1-k^2-n^2)}{(k^2+(1+n)^2)^2} + \frac{c1\, (8k^2+4n+4k^2n+8n^2+4n^3)}{(k^2+(1+n)^2)^2} \right) w^2 \mathrm{Sin}\left[\frac{d(-1+n)w}{c}\right]}{2}$$

3. Hessian Matrix, H_{22}

$$\frac{1280\, e^{-\frac{2dkw}{c}} k^2 (1+n)^2 \left(1-k^2-n^2\right)^2}{\left(k^2+(1+n)^2\right)^6} + \frac{80\, e^{-\frac{2dkw}{c}} (1+n)^2 \left(8k^2+4n+4k^2 n+8n^2+4n^3\right)^2}{\left(k^2+(1+n)^2\right)^6} +$$

$$\frac{1024\, e^{-\frac{2dkw}{c}} k^2 n (1+n) \left(1-k^2-n^2\right)}{\left(k^2+(1+n)^2\right)^5} - \frac{128\, e^{-\frac{2dkw}{c}} k^2 \left(1-k^2-n^2\right)^2}{\left(k^2+(1+n)^2\right)^5} -$$

$$\frac{32\, e^{-\frac{2dkw}{c}} (1+n) \left(4+4k^2+16n+12n^2\right) \left(8k^2+4n+4k^2 n+8n^2+4n^3\right)}{\left(k^2+(1+n)^2\right)^5} -$$

$$\frac{8\, e^{-\frac{2dkw}{c}} \left(8k^2+4n+4k^2 n+8n^2+4n^3\right)^2}{\left(k^2+(1+n)^2\right)^5} + \frac{128\, e^{-\frac{2dkw}{c}} k^2 n^2}{\left(k^2+(1+n)^2\right)^4} - \frac{64\, e^{-\frac{2dkw}{c}} k^2 \left(1-k^2-n^2\right)}{\left(k^2+(1+n)^2\right)^4} +$$

$$\frac{2\, e^{-\frac{2dkw}{c}} \left(4+4k^2+16n+12n^2\right)^2}{\left(k^2+(1+n)^2\right)^4} + \frac{2\, e^{-\frac{2dkw}{c}} (16+24n) \left(8k^2+4n+4k^2 n+8n^2+4n^3\right)}{\left(k^2+(1+n)^2\right)^4} -$$

$$2\, e^{-\frac{dkw}{c}} \left(-\frac{96\, c2\, k (1+n)^2 \left(1-k^2-n^2\right)}{\left(k^2+(1+n)^2\right)^4} + \frac{24\, c1 (1+n)^2 \left(8k^2+4n+4k^2 n+8n^2+4n^3\right)}{\left(k^2+(1+n)^2\right)^4} - \right.$$

$$\frac{64\, c2\, k n (1+n)}{\left(k^2+(1+n)^2\right)^3} + \frac{16\, c2\, k \left(1-k^2-n^2\right)}{\left(k^2+(1+n)^2\right)^3} - \frac{8\, c1 (1+n) \left(4+4k^2+16n+12n^2\right)}{\left(k^2+(1+n)^2\right)^3} -$$

$$\left. \frac{4\, c1 \left(8k^2+4n+4k^2 n+8n^2+4n^3\right)}{\left(k^2+(1+n)^2\right)^3} + \frac{8\, c2\, k}{\left(k^2+(1+n)^2\right)^2} + \frac{c1 (16+24n)}{\left(k^2+(1+n)^2\right)^2} \right) \mathrm{Cos}\left[\frac{d(-1+n)w}{c}\right] +$$

$$\frac{4\, d\, e^{-\frac{dkw}{c}} \left(-\frac{16\, c1\, k (1+n) \left(1-k^2-n^2\right)}{\left(k^2+(1+n)^2\right)^3} - \frac{4\, c2 (1+n) \left(8k^2+4n+4k^2 n+8n^2+4n^3\right)}{\left(k^2+(1+n)^2\right)^3} - \frac{8\, c1\, k n}{\left(k^2+(1+n)^2\right)^2} + \frac{c2 \left(4+4k^2+16n+12n^2\right)}{\left(k^2+(1+n)^2\right)^2} \right) w \mathrm{Cos}\left[\frac{d(-1+n)w}{c}\right]}{c}$$

$$+ \frac{2\, d^2\, e^{-\frac{dkw}{c}} \left(-\frac{4\, c2\, k \left(1-k^2-n^2\right)}{\left(k^2+(1+n)^2\right)^2} + \frac{c1 \left(8k^2+4n+4k^2 n+8n^2+4n^3\right)}{\left(k^2+(1+n)^2\right)^2} \right) w^2 \mathrm{Cos}\left[\frac{d(-1+n)w}{c}\right]}{c^2} +$$

$$2\, e^{-\frac{dkw}{c}} \left(\frac{96\, c1\, k (1+n)^2 \left(1-k^2-n^2\right)}{\left(k^2+(1+n)^2\right)^4} + \frac{24\, c2 (1+n)^2 \left(8k^2+4n+4k^2 n+8n^2+4n^3\right)}{\left(k^2+(1+n)^2\right)^4} + \right.$$

$$\frac{64\, c1\, k n (1+n)}{\left(k^2+(1+n)^2\right)^3} - \frac{16\, c1\, k \left(1-k^2-n^2\right)}{\left(k^2+(1+n)^2\right)^3} - \frac{8\, c2 (1+n) \left(4+4k^2+16n+12n^2\right)}{\left(k^2+(1+n)^2\right)^3} -$$

$$\left. \frac{4\, c2 \left(8k^2+4n+4k^2 n+8n^2+4n^3\right)}{\left(k^2+(1+n)^2\right)^3} - \frac{8\, c1\, k}{\left(k^2+(1+n)^2\right)^2} + \frac{c2 (16+24n)}{\left(k^2+(1+n)^2\right)^2} \right) \mathrm{Sin}\left[\frac{d(-1+n)w}{c}\right] +$$

$$\frac{4\, d\, e^{-\frac{dkw}{c}} \left(\frac{16\, c2\, k (1+n) \left(1-k^2-n^2\right)}{\left(k^2+(1+n)^2\right)^3} - \frac{4\, c1 (1+n) \left(8k^2+4n+4k^2 n+8n^2+4n^3\right)}{\left(k^2+(1+n)^2\right)^3} + \frac{8\, c2\, k n}{\left(k^2+(1+n)^2\right)^2} + \frac{c1 \left(4+4k^2+16n+12n^2\right)}{\left(k^2+(1+n)^2\right)^2} \right) w \mathrm{Sin}\left[\frac{d(-1+n)w}{c}\right]}{c}$$

$$\frac{2\, d^2\, e^{-\frac{dkw}{c}} \left(\frac{4\, c1\, k \left(1-k^2-n^2\right)}{\left(k^2+(1+n)^2\right)^2} + \frac{c2 \left(8k^2+4n+4k^2 n+8n^2+4n^3\right)}{\left(k^2+(1+n)^2\right)^2} \right) w^2 \mathrm{Sin}\left[\frac{d(-1+n)w}{c}\right]}{c^2}$$